Be and Bn stars: Balmer discontinuity and stellar-class relationship

Y. R. Cochetti, J. Zorec, L. S. Cidale, M. L. Arias, Y. Aidelman, A. F. Torres, Y. Frémat, A. Granada

A&A 634, A18 (2020)
https://doi.org/10.1051/0004-6361/201936444

Astronomy & Astrophysics

Be and Bn stars: Balmer discontinuity and stellar-class relationship*

Y. R. Cochetti[1], J. Zorec[2], L. S. Cidale[1,3], M. L. Arias[1,3], Y. Aidelman[1], A. F. Torres[1,3], Y. Frémat[2,4], and A. Granada[3,5]

[1] Departamento de Espectroscopía Estelar, Facultad de Ciencias Astronómicas y Geofísicas, Universidad Nacional de La Plata, La Plata, Argentina
e-mail: cochetti@fcaglp.unlp.edu.ar
[2] Sorbonne Université, CNRS, UPMC, UMR 7095, Institut d'Astrophysique de Paris, 98 bis bd. Arago, 75014 Paris, France
e-mail: zorec@iap.fr
[3] Instituto de Astrofísica de La Plata, CCT-La Plata, CONICET-UNLP, Paseo del Bosque s/n, CP 1900, La Plata, Buenos Aires, Argentina
[4] Royal Observatory of Belgium, 3 Av. Circulaire, 1180 Bruxelles, Belgium
[5] Laboratorio de Procesamiento de Señales Aplicadas y Computación de Alto Rendimiento, Sede Andina, Universidad Nacional de Río Negro, Mitre 630, San Carlos de Bariloche, R8400AHN Río Negro, Argentina

Received 2 August 2019 / Accepted 10 December 2019

ABSTRACT

Context. A significant number of Be stars show a second Balmer discontinuity (sBD) attributed to an extended circumstellar envelope (CE). The fast rotational velocity of Be stars undoubtedly plays a significant role in the formation of the CE. However, Bn stars, which are also B-type rapidly rotating stars, do not all present clear evidence of being surrounded by circumstellar material.
Aims. We aim to characterize the populations of Be and Bn stars, and discuss the appearance of the sBD as a function of the stellar parameters. We expect to find new indices characterizing the properties of CEs in Be stars and properties relating Be and Bn stars.
Methods. We obtained low- and high-resolution spectra of a sample of Be and Bn stars, derived stellar parameters, characterized the sBD, and measured the emission in the Hα line.
Results. Correlations of the aspect and intensity of the sBD and the emission in the Hα line with the stellar parameters and the $V \sin i$ are presented. Some Bn stars exhibit the sBD in absorption, which may indicate the presence of rather dense CEs. Six Bn stars show emission in the Hα line, so they are reclassified as Be stars. The sBD in emission appears in Be stars with $V \sin i \lesssim 250$ km s^{-1}, and in absorption in both Be and Bn stars with $V \sin i \gtrsim 50$ km s^{-1}. Low-mass Be and Bn stars share the same region in the Hertzsprung-Russell diagram. The distributions of rotational to critical velocity ratios of Be and Bn stars corresponding to the current stellar evolutionary stage are similar, while distributions inferred for the zero-age main sequence have different skewness.
Conclusions. We found emission in the Hα line and signs of a CE in some Bn stars, which motivated us to think that Bn and Be stars probably belong to the same population. It should be noted that some of the most massive Bn stars could display the Be phenomenon at any time. The similarities found among Be and Bn stars deserve to be more deeply pursued.

Key words. circumstellar matter – stars: emission-line, Be – stars: fundamental parameters

1. Introduction

Be stars are non-supergiant B-type stars that are rapidly rotating and surrounded by a gaseous extended circumstellar envelope (CE) whose structure and formation physics are still under debate. This envelope gives rise to a wide variety of spectroscopic peculiarities that characterize the Be phenomenon (see Porter & Rivinius 2003; Rivinius et al. 2013). Particularly, in the optical range Be stars show, or have shown at least once, hydrogen lines in emission (Jaschek et al. 1981). Their continuum spectra exhibit flux excesses mainly in the optical and near-infrared regions and, in several cases, they exhibit two components of the Balmer discontinuity (BD; Barbier & Chalonge 1939; Chalonge & Divan 1952; Schild 1978; Divan 1979). The first component of the BD, D^*, is stellar photospheric. It is constant and defines the spectral type of the stellar hemisphere projected toward the observer, as it does for emissionless non-supergiant B-type stars. The second component of the BD (sBD, d) appears at shorter wavelengths, very close to the theoretical Balmer line series limit. This second component of the BD originates in a low pressure stellar gaseous environment. It is variable and can be either in emission or in absorption. At times, it can completely disappear (e.g., Divan 1979; Underhill & Doazan 1982; Zorec 1986; Zorec & Briot 1991; Moujtahid et al. 1998; Aidelman et al. 2012).

Schild (1978), Kaiser (1987, 1989) and Dachs et al. (1989) presented a series of papers with measurements of d for a reduced number of northern and southern non-shell Be stars. These authors found trends or vague correlations between d and the emission in the Hα line. Indirect indications of the existence of a relationship between the total BD, $D = D^* + d$ (sometimes called anomaly of the BD), and the emission in the Balmer lines were also put forward by Feinstein & Marraco (1979) and Peton (1981). Divan et al. (1982) obtained a correlation between d and the Balmer decrement. Since then scarce observational programs

* Based on observations obtained at the Complejo Astronómico El Leoncito (CASLEO), operated under an agreement between the Consejo Nacional de Investigaciones Científicas y Técnicas de la República Argentina, the Secretaría de Ciencia y Tecnología de la Nación and the National Universities of La Plata, Córdoba and San Juan, Argentina.

were carried out to study the appearance of the sBD. Apart from the models of CE by Poeckert & Marlborough (1978a,b), where the sBD appears as a marginal phenomenon at extremely high CE densities, Moujtahid et al. (1999) and Cruzado & Zorec (2009) presented discussions on the behavior of the sBD and concluded that its appearance depends on the density distribution in the CE, its temperature, and inclination angle.

Knowing that the study of the appearance of the sBD could help us better understand the physical nature of the Be phenomenon, it is tempting to start a systematic study of the BD to uncover still unknown or perhaps unsuspected characteristics of the CE near the central star. Hence, the main goals of the present work are to analyze the frequency of appearance of the sBD as well as its aspect and intensity as functions of the stellar fundamental parameters in a sample of Be stars as large as possible.

In the Bright Star Catalogue (BSC; Hoffleit & Jaschek 1982), a non-negligible number of B and A stars are named Bn, An, but also Bnn and Ann stars. Their spectra are characterized by the hydrogen Balmer lines, lines of neutral helium, and lines of singly ionized oxygen, iron, and other gases that define the respective classical MK (Morgan & Keenan 1973) B and A spectral type-luminosity classes. Most of these stars are in the B7-A2 range of spectral types. To the known MK spectral type designation, Adams & Joy (1923) added the tag "n" to indicate that the spectroscopic lines (mostly metallic) are "nebulous" in contrast to sharper lines observed in other stars (Ghosh et al. 1999). In general, "n" stands for broad absorption lines, and "nn" for very broad absorption lines. It is presumed that the broad aspect of these lines is due to the stellar rapid rotation. In contrast to Be stars, Bn stars do not show any emission component in hydrogen and other lines. In a search for rapid *ubvy* photometric variations in southern Be and Bn stars, Barrera et al. (1991) found that the amplitude of changes in Bn stars rarely exceed 0.02 mag.

Rapid rotation is a unifying property of the Be star group and certainly has a significant impact on the production of the Be phenomenon (cf. Zorec et al. 2016, and references therein). However, Bn stars also show very high rotation rates. If we assume that the broad and shallow spectral lines of Bn stars are due to rapid rotation, these stars would be observed equator-on. Rapidly rotating stars seen pole-on may also exist, but because of the lack of rotation-related features, we cannot identify these stars as rapid rotators. To our knowledge, there is no citation in the current literature to systematic research of gravity darkening-related (GD) signatures in the metallic lines of normal B-type stars with sharp lines, as is now being carried out for pole-on A-type stars (Royer et al., in prep.).

The frequency of Be stars has two maxima: one at B1-B2 spectral type and a secondary one at B5 spectral type (Zorec & Briot 1997), mostly as a consequence of the combination of the behavior of the source function of Balmer lines with the effective temperature and the shape of the initial mass function (IMF; Zorec et al. 2007a). Contrarily, Bn stars are mainly main-sequence (MS) stars of late B spectral type that seem to complete an apparent statistical lack of Be stars at these effective temperatures (Zorec 2000; Zorec et al. 2007a). Since only a few Bn stars have been observed with some emission in the Balmer lines (Ghosh et al. 1999; Rivinius et al. 2006), it is legitimate to ask whether Bn stars possess weakly developed circumstellar disks, or whether they have attained the required (unknown) physical properties to become full-fledged Be stars (Zorec et al. 2005). Gkouvelis et al. (2016) produced a simple model of circumstellar disk in Be stars to study the uncertainties affecting the aspect of the first BD due to the presence of the sBD and the intrinsic reddening of the Paschen continuum. As a by-product of this discussion, the authors show that the sBD can easily appear in late B-type stars with low-density CE. However, they are not able to raise sizeable emission signatures at least in the spectral lines, mainly Hα, to reveal the presence of a circumstellar disk.

Given these cited facts, we include Bn stars to the present study, not only as a function of fundamental parameters ($T_{\rm eff}$, $\log g$, $\log L/L_{\odot}$) which have been scarcely determined, but also to study these objects, on one hand in the frame of rapid rotation to search for links between Be and Bn stars, and on the other hand as incipient builders of CEs. We note the role of rotation in the incidence of the Be phenomenon. Based on a detailed analysis of rotational speeds for a large sample of Be stars, Zorec et al. (2016) conclude that most of these stars rotate at $V/V_{\rm c} \simeq 0.65$ and that the probability is low that these stars are critical rotators. This means that Bn stars probably do not need to become critical rotators to develop low-density CEs. However, there remains a question as to whether Be and Bn stars are differential rotators with critical or near-critical equatorial rotation, but we observe these stars as having an average global under critical linear velocity parameter V because we get integrated radiation over the stellar hemisphere (Zorec et al. 2017a,b).

In the present paper we present observational characteristics of Be and Bn stars mainly based on the behavior of their sBD and rotational velocities. A discussion on a possible stellar-class relationship between Be and Bn stars is then included.

Because the sBD is related to the presence of a CE, in a second paper of these series we will produce a model to test the required properties of the CE to give rise to this feature with its observed characteristics to uncover or emphasize additional links between Be and Bn stars.

2. Observational data

Our sample consists of 66 Be and 61 Bn Galactic stars, listed in the BSC (Hoffleit & Jaschek 1982). Low- and high-resolution spectroscopic observations for the sample stars were obtained at the Complejo Astronómico El Leoncito (CASLEO), San Juan, Argentina. In addition, we obtained Hα spectra for some Be stars from the Be Star Spectra database (BeSS; Neiner et al. 2011) or the Spectroscopic Be Stars Atlas[1]. We particularly searched for available spectra taken at dates as close as possible to that of our low-resolution observations.

In Tables A.1 and A.2 we give, for Be and Bn stars, respectively, the HD number of each observed star, star coordinates, apparent visual magnitude, and dates of observation. For some targets we obtained observations in two different epochs.

All the low-resolution CASLEO observations were carried out using the Boller & Chivens Cassegrain spectrograph attached to the *Jorge Sahade* telescope. Except for the 2004 spectra, the instrumental configuration consisted of a 600 ℓ/mm grating, a slit width of 250 μm, and a TEK 1024 CCD detector. The covered spectral range was 3500–5000 Å and the effective resolution 5.25 Å every two pixels ($R \approx 660$). For 2004 observations another CCD detector was used (PM 512), resulting in an effective resolution of 4.53 Å every two pixels ($R \approx 900$) and a little shorter spectral range (3500–4600 Å). Accompanying high-resolution spectra were obtained using the Recherches et Études d'Optique et de Science Connexes (REOSC) spectrograph, attached to the same telescope, in cross-dispersion mode with a 400 ℓ/mm grating, a slit width of 250 μm, and a 1024×1024 CCD detector. The observed spectral range is 4200–6700 Å with $R \approx 12\,600$.

[1] http://www.astrosurf.com/buil/us/becat.htm

The CASLEO observations were reduced using the IRAF[2] software package and applying a standard reduction procedure. Bias, flat-field, He-Ne-Ar comparison, and spectrophotometric flux standard star spectra were secured to perform bias and flat-field corrections along with wavelength and flux calibrations for the low-resolution spectra. For the high-resolution spectra we used a Th-Ar Lamp as a comparison spectra. High-resolution spectra were not flux calibrated, and all the spectra were corrected for atmospheric extinction.

2.1. BCD spectrophotometry

2.1.1. First component of the BD

The BCD spectrophotometric classification system (see basic definitions in Barbier & Chalonge 1941; Chalonge & Divan 1952; Zorec & Briot 1991) is based on measurements of the BD in low-resolution spectra observed in the 3400–4600 Å wavelength range. The photospheric component of the BD is characterized by the parameter D^*, which is given by the log of the ratio of the Paschen to Balmer continuum flux extrapolated at 3700 Å , $D^* = \log(F_{+3700}/F_{-3700})$, and is a strong indicator of the stellar effective temperature, $T_{\rm eff}$. The flux $\log F_{+3700}$ is determined by extrapolating at λ 3700 Å the rectified Paschen continuum flux $\log F_\lambda$. The value of $\log F_{-3700}$ is determined by the conjunction of the upper and lower wraparound curves of the last absorption lines of the Balmer series, as shown in Fig. 1. The parameter λ_1 is the mean spectral position of the Balmer jump, relative to λ 3700 Å, and provides a good indication of the stellar surface gravity, $\log g$. It is determined by the intersection of the line parallel to the Paschen continuum that passes through the point $(3700, \log F_{+3700} - D^*/2)$ (dotted line in Fig. 1) and the upper wraparound curve of the last members of the Balmer line series.

The measurement of the BCD parameters was performed with an interactive code developed by one of us (Y.A.) and successfully implemented to study B stars in open clusters (Aidelman et al. 2012, 2015, 2018). Typical uncertainties of these quantities are $\sigma(D^*) \lesssim 0.015$ dex and $\sigma(\lambda_1) \sim 3$Å. The BCD (λ_1, D^*) parameters allow us a straightforward determination of the spectral type and the luminosity class of stars, as well as of the stellar parameters (Zorec et al. 2009). In general, the spectral types based on the BCD stellar parameters of emissionless stars are in agreement with the MK classification within one to two subtypes.

Tables A.3 and A.4 list the (λ_1, D^*) parameters in Cols. 2 and 3, and the corresponding spectral types and luminosity classes determined in this work (Col. 4) of the program Be and Bn stars, respectively. Six objects of our sample: HD 31209, HD 42327, HD 43445, HD 165910, HD 171623, and HD 225132, considered up to now as Bn stars, turned out to have an emission component in their Hα line, so they are included in the Be star sample.

Figure 2 shows the BCD (λ_1, D^*) version of the Hertzsprung–Russell (HR) diagram of the studied Be and Bn stars. This diagram shows that the BCD parameters (λ_1, D^*) have high precision in both spectral type and luminosity class. In some particular cases, when emission is very strong, mostly among the hottest stars (from O8- to B1-type), the BCD spectral types can be somewhat earlier than expected (around half spectral type). This happens because the emission in the sBD can slightly overlap the photospheric emission, when the continuum flux excess and the emission in the spectral lines are very strong. However, the separation between the photospheric and circumstellar Balmer discontinuities is clear for all the remaining cooler spectral types. On one hand, because of this separation and because the parameter D^* is determined by a ratio of fluxes at the same wavelength ($\lambda = 3700$ Å), this quantity is independent of the circumstellar perturbing emission and absorption, and its dependence with the interstellar extinction is only of second order, through the slope of the Paschen energy distribution, $\log F_\lambda$, which is on the order of $\delta D^* \lesssim 0.01 E(B-V)$ dex. On the other hand, the λ_1 parameter is independent of both the interstellar extinction and the circumstellar absorption and emission. Our sample of Be stars has luminosity classes in the V-II range, while the Bn stars show luminosity classes V or IV.

Figure 3 shows the occurrence histogram of the frequency of spectral types in the Be and Bn stellar sample studied using the BCD system. In this figure the maximum frequency of Be stars is located around the B2 spectral type, in agreement with that reported by other authors for other samples of Be stars (e.g.,

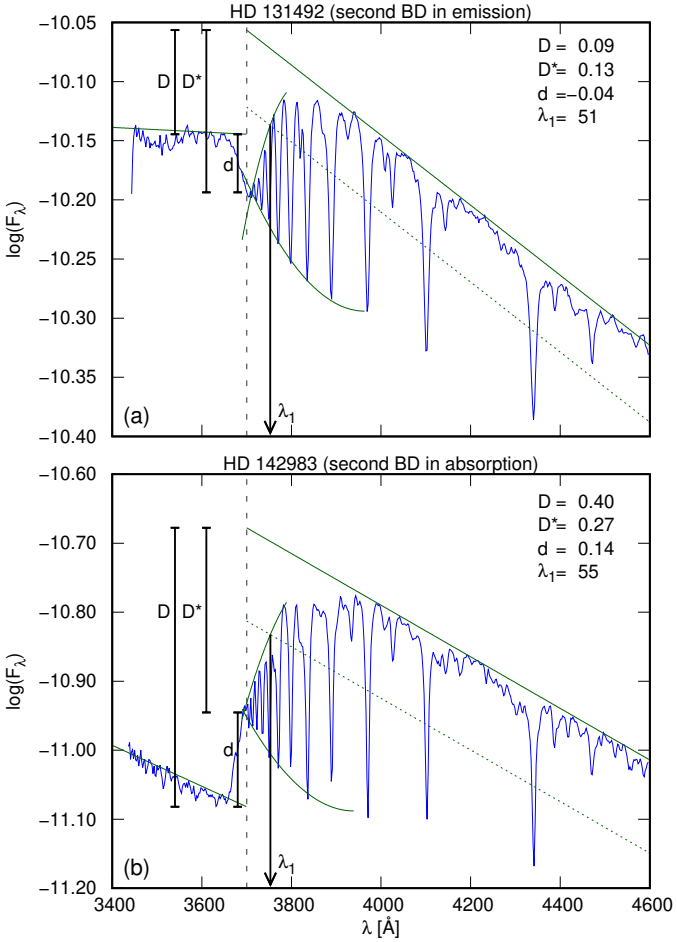

Fig. 1. Low-resolution spectra for two different Be stars illustrating the cases for sBD in absorption and in emission. The different components of the BD are indicated: D (total), D^* (photospheric), and d (circumstellar). The straight green lines at $\lambda > 3700$ Å and $\lambda < 3700$ Å represent the rectified Paschen and Balmer continuum flux. The vertical dashed line indicates the wavelength λ 3700 Å at which the flux ratios are measured. The dotted green line represents $\log F_{+3700} - D^*/2$, and is used to determine the λ_1 parameter, whose abscissa is indicated with a vertical arrow (see Sect. 2.1.1.).

[2] IRAF is distributed by the National Optical Astronomy Observatory, which is operated by the Association of Universities for Research in Astronomy (AURA) under cooperative agreement with the National Science Foundation.

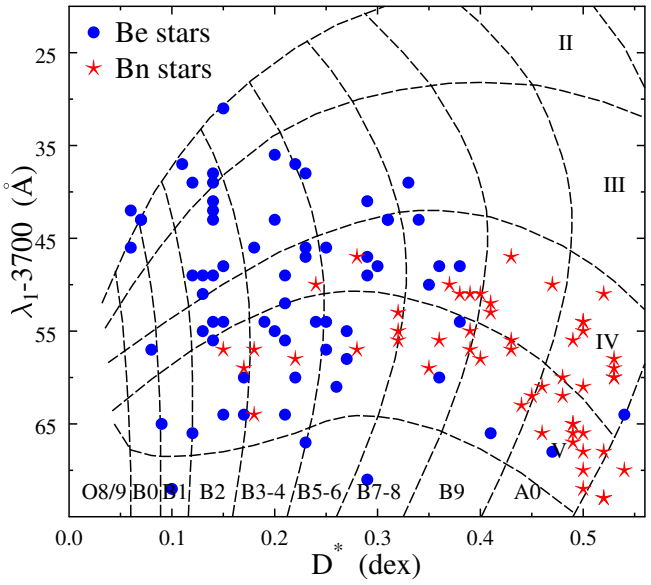

Fig. 2. Calibration of the BCD (λ_1, D^*) plane in terms of the MK spectral type. The vertical dashed lines show the limits of the MK spectral type groups indicated on the axis of abscissas. The horizontal dashed lines represent the limits of the MK luminosity classes, which are indicated in the last vertical curvilinear quadrilaterals. Our sample of Be stars has luminosity classes in the V-II range, while the Bn stars show luminosity classes V or IV.

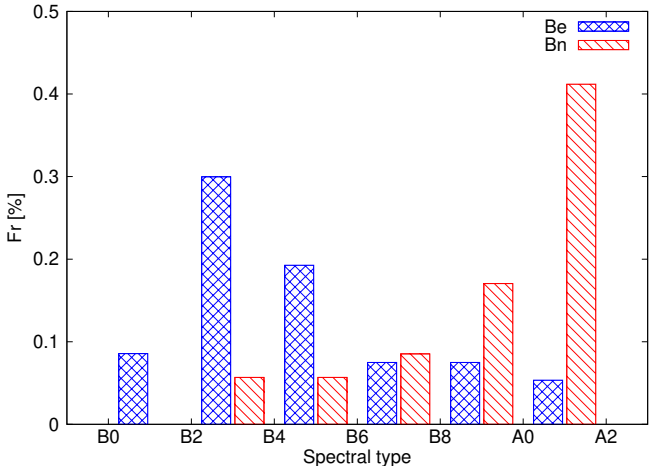

Fig. 3. Histogram of BCD spectral types of the studied Be and Bn stars. The maximum frequency of Be stars is located around the B2 spectral type. The number of Bn stars strongly increases toward late B and early A-type spectral types. Both Be and Bn stars spread over the entire range of B-type stars.

Jaschek & Jaschek 1983; Zorec & Briot 1991). As already noted in the introduction, the number of Bn stars strongly increases toward late B and early A-type spectral types. Nevertheless, it is interesting to note that both Be and Bn stars spread over the entire range of B-type stars.

2.1.2. Second Balmer discontinuity

One of the objectives pursued in this work is to characterize the sBD component in a rather large sample of Be and Bn stars. In general, Be stars can have a BD with two components. One of these components (D^*, mentioned in Sect. 2.1.1) characterizes the photosphere of the rotationally deformed stellar hemisphere

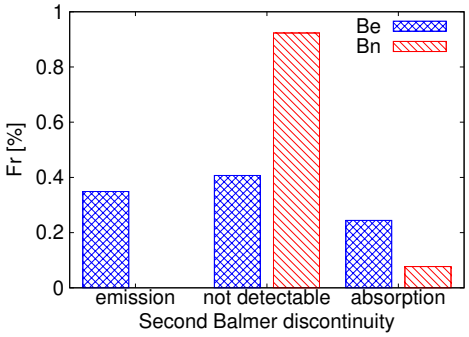

Fig. 4. Diagram showing the frequency of appearance of the sBD in our Be and Bn stellar sample. More than half of the Be stars in our sample present the sBD either in emission or in absorption. The fraction of Bn stars that present the sBD in absorption is small.

projected toward the observer, and the second (d) is produced by the circumstellar gaseous environment of these objects. We refer then to a total BD written as $D = D^* + d$ dex. According to the definition put forward by Divan (1979), when the sBD is in emission we have $d < 0$, and $d > 0$ when it is in absorption. In Fig. 1 we show examples of spectra with the sBD in emission (top) and in absorption (bottom), and where the determination of D, D^*, and d is indicated.

Once those Bn stars for which we found an emission component in the Hα line were moved to the Be star group, the Be and Bn star samples were left with 73 and 55 objects, respectively. Among the 73 Be sample stars, 38 have a measurable sBD, 23 of which are in emission and the other 15 in absorption. In 13 spectra of the whole sample, we see an incipient sBD, but it is too small to be measured reliably. Seven of these spectra present $d \lesssim 0$ and the other six $d \gtrsim 0$. In all remaining Be stars only the first BD is seen. Regarding the Bn stars, 3 out of 55 stars show a measurable sBD in absorption, and other two spectra present $d \gtrsim 0$, but they are too tiny to be measured with certainty. In the remaining spectra of Bn stars there is no detectable sBD. A graphical summary of the fraction of stars versus the aspect of the sBD for Be and Bn stars is presented in Fig. 4.

The measured values of the sBD, d, are given in Col. 5 of Tables A.3 and A.4 for Be and Bn stars, respectively, where d values range from −0.07 dex to 0.14 dex for Be stars and from 0.00 dex to 0.03 dex for Bn stars. For those objects with two measurements of d, we present both values. The text "em" or "abs" in the d column indicates those cases in which the sBD is too small to be measured reliably.

2.2. Hα line observations for program Be and Bn stars

2.2.1. Be stars

In this section we present our Hα observations for the program Be stars. Figures 5 and 6 show the Hα line profiles for the stars without and with a sBD, respectively. In Fig. 6, the top panel shows the spectra for objects with $d < 0$ while the lower panel corresponds to those with $d > 0$, including the stars for which the sBD is too small to be measured with certainty. In both figures, the symbol * stands for those spectra taken from the already mentioned databases. We note that HD 209014 has been seen once with $d > 0$ and another time without a sBD.

In our search for Be stars that show a clear sBD, we have preferentially chosen those with strong Hα emission, based on the correlations given in Divan et al. (1982). Unfortunately, this may contribute with some biased effects on the aspect

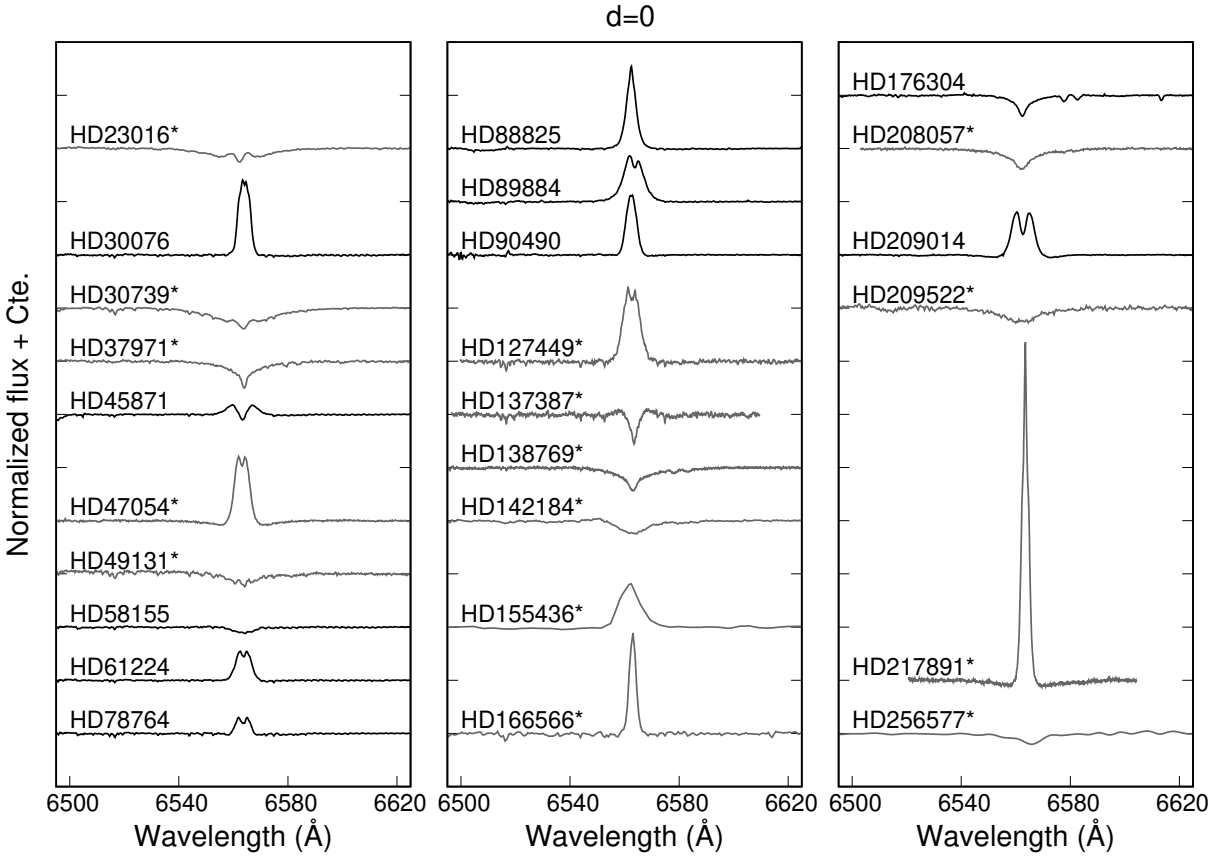

Fig. 5. Hα line profiles belonging to the program Be stars without a sBD, observed at dates close to that of our low-resolution observations. Spectra with the * symbol were downloaded from the BeSS database (Neiner et al. 2011) or the Spectroscopic Be Stars Atlas (`http://www.astrosurf.com/buil/us/becat.htm`).

angle statistics carried in later sections of this work. Indeed, we selected stars with rather low aspect angles, which likely display stronger emissions due to the CE.

It is worth mentioning that for HD 35411, the upper Hα line profile in Fig. 6, that presents a small emission above the photospheric absorption, have been taken around three years before our first low-resolution spectrum with the sBD in emission. Also, the other Hα line profile is for the same month of our second low-resolution spectrum, but does not show evidence for an emission component, expected due to the sBD in emission. It is possible that the development of a CE was recent. On the other hand, HD 187811 shows a Hα line profile with a weak double-peaked shell-like emission overimposed to the photospheric absorption. This spectra was taken almost four months before our low-resolution spectrum with a sBD in absorption. Considering the spectral variability of this object (Mennickent et al. 2009; Vieira et al. 2017; Sabogal et al. 2017), it is possible that the small emission in the Hα line occurred owing to the development of a new CE that was present when the sBD was observed.

In Fig. 6 ($d > 0$, bottom panel) the Hα profiles of the six newly discovered Be stars, which were previously classified Bn stars, are included. For HD 31209 and HD 171623, the Hα line profiles has a shell-like double-peaked weak emission cutting the bottom of the underlying photospheric absorption. In HD 43445 and HD 225132, the Hα profiles show shell-like intense double-peaked emission superimposed on the photospheric absorption. In HD 42327 we see a particularly rounded bottom of the line absorption possibly due to some emission that partially fills up the underlying photospheric absorption component. In HD 165910, however, there is an extra absorption in the bottom of the photospheric component, which is typical for B-shell stars (Hubert-Delplace & Hubert 1979).

2.2.2. Bn stars

We obtained high-resolution Hα spectra for those program Bn stars that present (or might present) a sBD. Since the sBD is most probably originated by a more or less extended envelope around the star, we expected to detect emission in the Hα line as well.

As mentioned in Sect. 2.1.1, six stars previously classified as Bn stars have been included in the Be star group because they show emission components or shell-like absorptions in their Hα line profiles. These stars are considered in this paper as genuine Be stars and were included in the Be star group.

In Fig. 7 we show the Hα line profiles for those Bn stars with an indication of a possible sBD in their low-resolution spectra. All the line profiles have a photospheric-like aspect. However, to determine whether they are affected by some emission or extra absorption produced by the CE, it is still necessary to fit theoretical profiles to simultaneous high-resolution observation in the blue (Hγ, Hδ, Hϵ lines) and red (Hα) spectral ranges. Differences between observed and modeled Hα line profiles could finally determine whether there is some CE emission or extra absorption.

The rapid rotation that characterizes Bn stars, the occasional appearance of some emission in the Balmer lines (at least in Hα), and the presence of signatures for some sBD are motivate us to think that Bn and Be probably belong to the same class of objects. Some attempts to show a possible correlation between

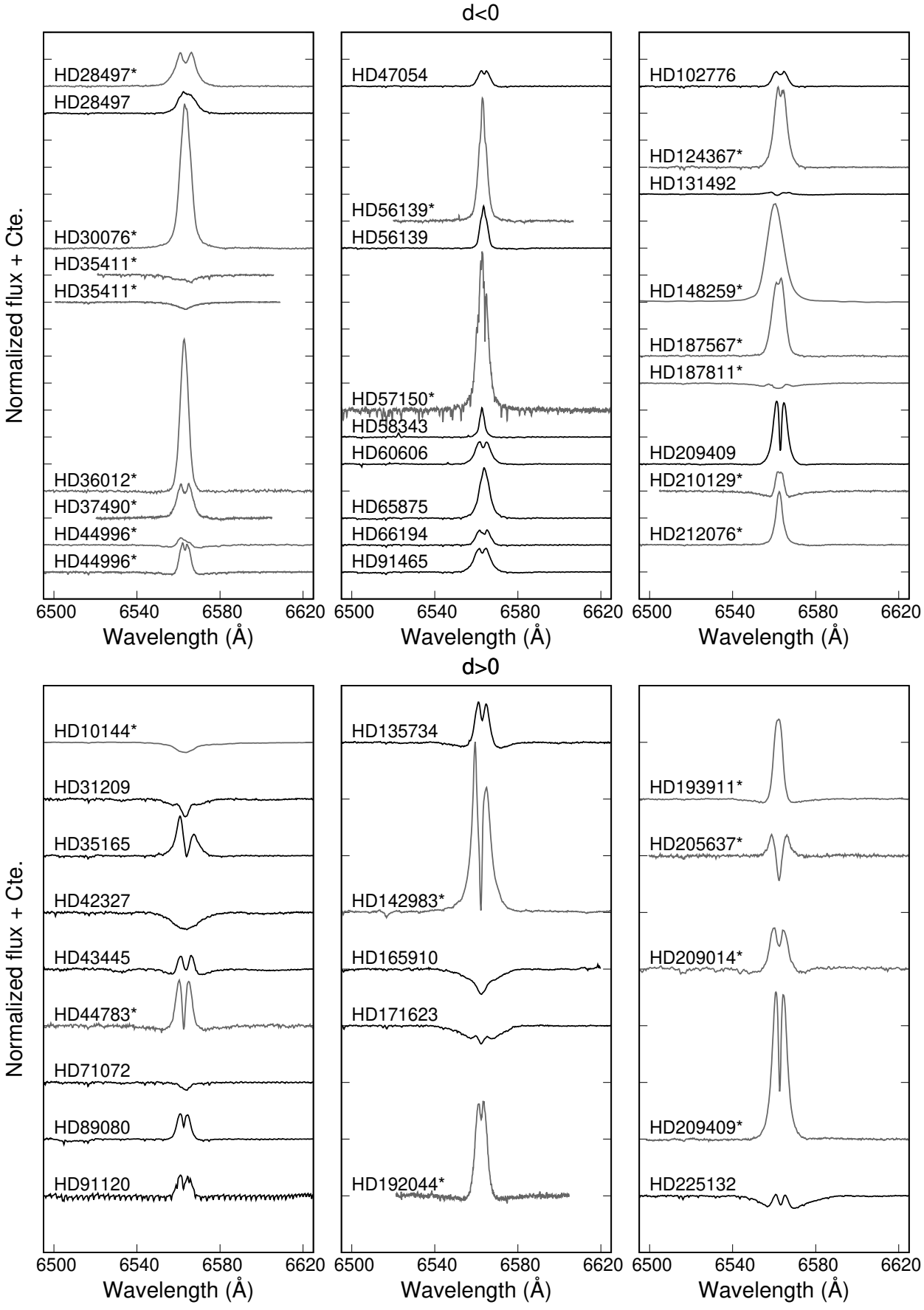

Fig. 6. Hα line profiles belonging to the program Be stars with sBD in emission ($d < 0$, *top panels*) and in absorption ($d > 0$, *bottom panels*), observed at dates close to those of our low-resolution observations. Spectra with the * symbol were downloaded from the BeSS database (Neiner et al. 2011) or the Spectroscopic Be Stars Atlas (http://www.astrosurf.com/buil/us/becat.htm).

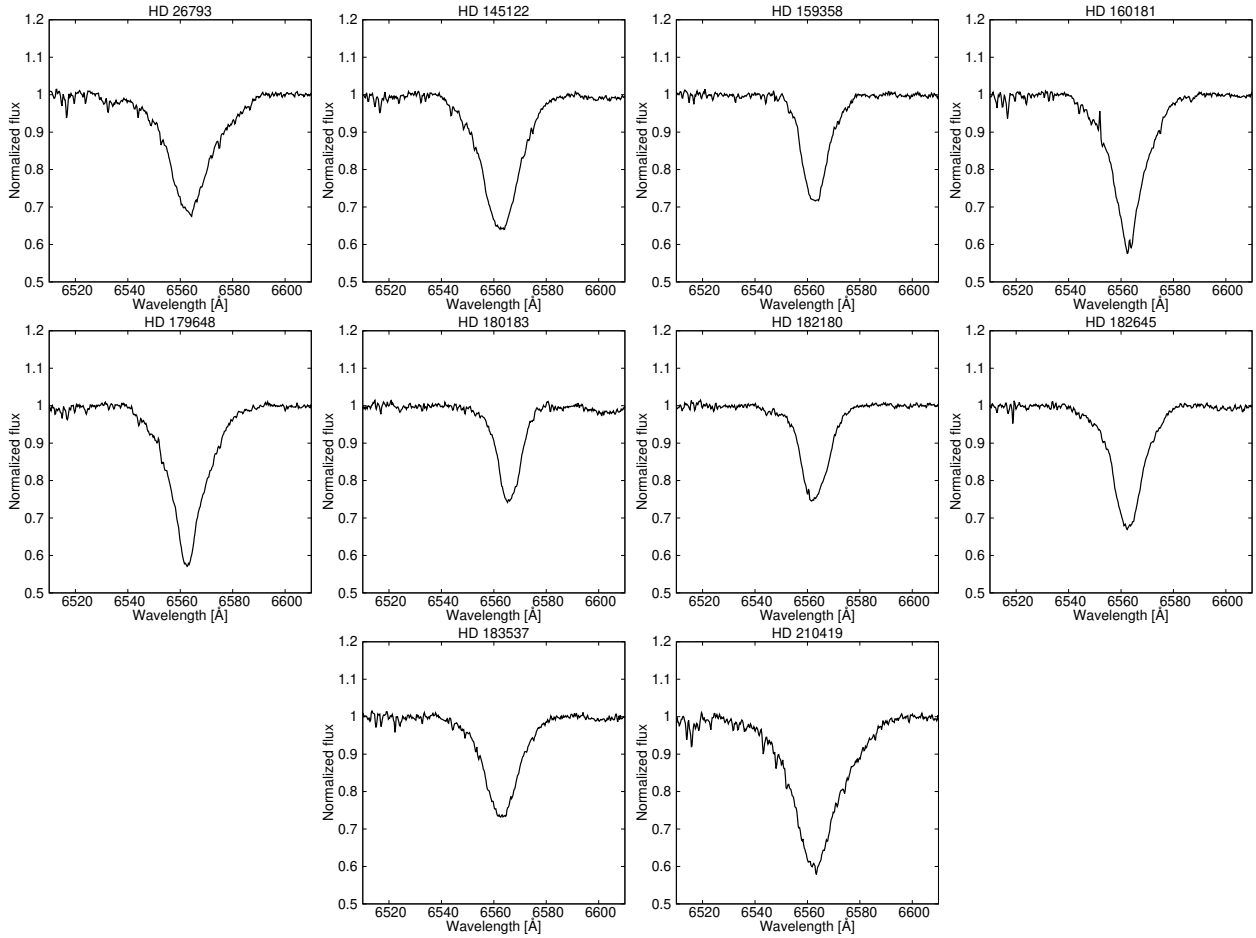

Fig. 7. Hα line for Bn stars that present a sBD, including the stars for which the sBD is too small to be measured with certainty. These profiles have a photospheric-like absorption aspect.

fast-rotating late B-type stars and Be stars based on the presence of a sBD were discussed by Aidelman et al. (2018) in open clusters.

2.3. *V*sin *i* parameters

With the purpose of searching for physical reasons that could justify class relations between Be and Bn stars, we compiled $V\sin i$ parameters of the program stars published in the literature or determined in this work. The $V\sin i$ values were taken from Chauville et al. (2001), Zorec et al. (2005), Frémat et al. (2005) and Zorec & Royer (2012). We also adopted values from Dworetsky (1974), Slettebak (1982), Uesugi & Fukuda (1982), Wolff et al. (1982), Brown & Verschueren (1997), Yudin (2001), Abt et al. (2002), Strom et al. (2005), Levenhagen & Leister (2006) and Díaz et al. (2011). For three of the program stars we did not find any $V\sin i$ determinations nor the required spectra to be able to measure them. The finally adopted values of $V\sin i$ and their uncertainties are listed in Cols. 13 and 14 of Tables A.3 and A.4. Column 15 of these tables indicates the respective references.

3. Second Balmer discontinuity and the inclination angle of the rotation axis

In several occasions, evidence was put forward to claim that flux excesses representing either emission or absorption in the visible continuum spectrum of Be stars should be produced in circumstellar disk layers laying close to the central star (Moujtahid et al. 1998, 1999, 2000). This suggestion seems to be supported by recent calculations of the visual energy distribution in Be stars based on models of viscous CE (Carciofi & Bjorkman 2008; Haubois et al. 2012; Klement et al. 2017).

Knowing that most Be stars show a sBD either in emission or absorption, we are tempted to ask whether there is a relationship between the inclination angle and the geometry of the CE. Nevertheless, it is worth noting that a few cases were reported in the literature in which the genuine Be aspect of the Hα line remained unchanged over a long period of time and then changed to a genuine Be-shell aspect or the line emission or extra absorption component simply disappeared for a while. The sBD might then also change from emission to absorption or simply disappear (Hirata & Kogure 1977; Moujtahid et al. 1999). In these particular cases, finding this kind of relationship might be somewhat challenging.

In this section, we carried out statistical tests to determine the observational circumstances under which the sBD appears by trying to infer the ranges of inclination angles at which it may appear in emission or in absorption. Knowing that the $V\sin i$ parameters are currently underestimated owing to the GD effect (Stoeckley 1968; Townsend et al. 2004; Frémat et al. 2005; Zorec et al. 2016), to obtain a rough first insight on the inclination angles we corrected the projected rotational velocities, assuming that all the studied stars rotate on average at the same angular velocity ratio $\Omega/\Omega_c = 0.95$; this ratio closely corresponds to the average ratio $\eta = 0.6$ of equatorial centrifugal to gravitational

forces characterizing a large sample of Be stars near the Sun (Zorec et al. 2016).

We call $\langle V\sin i\rangle_{\rm em}$ the average $V\sin i$ parameter that corresponds to those program Be stars with the sBD in emission, and $\langle V\sin i\rangle_{\rm abs}$ the average characterizing the Be stars with the sBD in absorption. Admitting that the circumstellar gaseous structures around Be stars are globally flattened, we can think of a sBD in emission from objects that are preferentially seen at inclination angles from $i=0^\circ$ to some $i=I_{\rm em}$, while the sBD in absorption is detected in stars having aspect angles from some $i=I_{\rm abs}$ to $i=90^\circ$. The distribution function of the actual linear velocity V and that for the inclination angle i are independent. Since $\sin i\,{\rm d}i$ is the probability of finding an object inclined between the angles i and $i+di$, the $\langle V\sin i\rangle_{\rm em,abs}$ averages are formally given by

$$\begin{aligned}\langle V\sin i\rangle_{\rm em} &= \langle V\rangle\frac{\int_0^{I_{\rm em}}\sin^2 i\,{\rm d}i}{\int_0^{I_{\rm em}}\sin i\,{\rm d}i}\\ &= \frac{\langle V\rangle}{2}\left(\frac{I_{\rm em}-\frac{\sin 2I_{\rm em}}{2}}{1-\cos I_{\rm em}}\right)\\ \langle V\sin i\rangle_{\rm abs} &= \langle V\rangle\frac{\int_{I_{\rm abs}}^{\pi/2}\sin^2 i\,{\rm d}i}{\int_{I_{\rm abs}}^{\pi/2}\sin i\,{\rm d}i}\\ &= \frac{\langle V\rangle}{2}\left(\frac{\frac{\pi}{2}-I_{\rm abs}+\frac{\sin 2I_{\rm abs}}{2}}{\cos I_{\rm abs}}\right),\end{aligned}\tag{1}$$

where $\langle V\rangle$ is the average of all true rotational velocities of the entire Be star sample. In a similar way, the average angles $\langle i_{\rm em}\rangle$ and $\langle i_{\rm abs}\rangle$ under which are seen the sBD in emission or absorption are functions of $I_{\rm em}$ and $I_{\rm abs}$, respectively, given by

$$\begin{aligned}\langle i_{\rm em}\rangle &= \frac{\int_0^{I_{\rm em}} i\,\sin i\,{\rm d}i}{\int_0^{I_{\rm em}}\sin i\,{\rm d}i} = \frac{\sin I_{\rm em}-I_{\rm em}\cos I_{\rm em}}{1-\cos I_{\rm em}}\\ \langle i_{\rm abs}\rangle &= \frac{\int_{I_{\rm abs}}^{\pi/2} i\,\sin i\,{\rm d}i}{\int_{I_{\rm abs}}^{\pi/2}\sin i\,{\rm d}i} = \frac{1+I_{\rm abs}\sin I_{\rm abs}}{\cos I_{\rm abs}}.\end{aligned}\tag{2}$$

In Tables A.3 and A.4, the adopted apparent $V\sin i$ values with their uncertainties as reported in the literature are given in Cols. 13 and 14 (for definition of apparent fundamental parameters, see Frémat et al. 2005; Zorec et al. 2016). Assuming that these uncertainties correspond to the standard deviation of the individual estimates, we carried out 10^4 Monte Carlo bootstrapped trials to calculate the averages $\langle V\sin i\rangle_{\rm em,abs}$ defined in Eq. (1) and estimated the respective inclination angles $I_{\rm em}$ and $I_{\rm abs}$ and their corresponding averages given in Eq. (2). The normalized distributions of $I_{\rm em,abs}$ and $\langle i_{\rm em,abs}\rangle$ thus obtained are shown in Fig. 8. In this figure, the histograms in full lines show that the values of $I_{\rm em}$ and $I_{\rm abs}$ spread over large intervals of inclination angles owing to the uncertainties of the individual $V\sin i$ parameters. The histograms drawn with dashed lines correspond to the distributions of $\langle i_{\rm em}\rangle$ and $\langle i_{\rm abs}\rangle$ that indicate at what angles we can expect to observe the sBD in emission and in absorption, respectively. The arrows indicate the domains over which the integrations that define $\langle i_{\rm em,abs}\rangle$ were performed, respectively.

The results shown in Fig. 8 indicate that according to the observed averages $\langle V\sin i\rangle_{\rm em}$ there must be stars with a sBD in emission observed at inclination angles $I_{\rm em}\lesssim 70^\circ$, while the absorption in the sBD should be displayed in stars that have inclination angles $I_{\rm abs}\gtrsim 60^\circ$. Since the extra emission or absorption

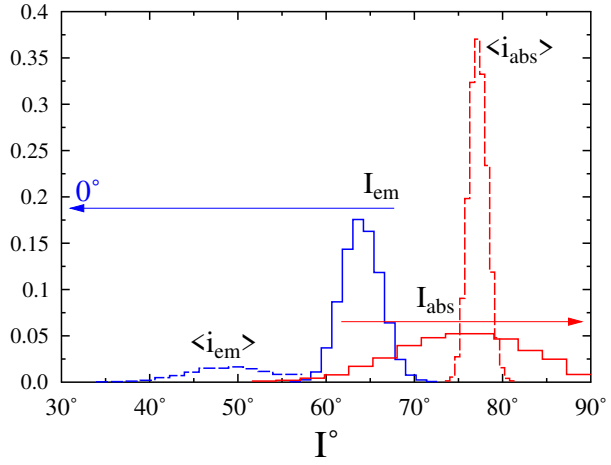

Fig. 8. Full lines: histograms of Monte Carlo simulations for limit inclinations $I_{\rm em,abs}$ defined in Eq. (1). Dashed lines: histograms of average angles $\langle i_{\rm em,abs}\rangle$ defined in Eq. (2). Blue indicates stars with sBD in emission, red indicates sBD in absorption. The arrows indicate the domains over which the integrations that define $\langle i_{\rm em,abs}\rangle$ were performed, respectively.

in the continuum spectrum produced by the CE detected as a sBD cannot come from circumstellar layers situated too far from the central star, our statistical inferences suggest that the CEs must have high enough vertical optical depths in these regions; this is very similar to suggestions made sometime ago by Arias et al. (2006) and Zorec et al. (2007b) to account for the presence of Fe II emission lines originating in CE layers that are near the central star. The rather significant vertical height of CE layers near the star is also supported by the fact that rarely the sBD appears at wavelengths that are larger than the theoretical limit of Balmer lines series, λ3648 Å (Divan 1979; Zorec & Briot 1991; Moujtahid et al. 1999; Gkouvelis et al. 2016), where the electron density of the CE layers close to the central star cannot be larger than some $N_{\rm e}\sim 10^{13}$ cm^{-3}. Otherwise the sBD would heavily encroach upon the first or photospheric BD, phenomenon that was exceptionally observed during some emission phases. Thus, to attain optical depths $\tau\lesssim 1$ in the visible continuum spectrum in CE layers close to the central star that produce a sBD, the CE should have a high enough vertical height.

4. Apparent and parent nonrotating counterpart parameters

4.1. Apparent parameters

In our vocabulary, the observed quantities are considered as "apparent" parameters. The observed BCD (λ_1, D^*) quantities are then apparent, but also all those which are derived or read in their calibrations, like the effective temperature $T_{\rm eff}(\lambda_1, D^*)$, visual absolute magnitude $M_{\rm V}(\lambda_1, D^*)$, and bolometric absolute magnitude $M_{\rm bol}$ (Divan & Zorec 1982; Zorec 1986; Zorec & Briot 1991; Zorec et al. 2009). A description of these calibrations can also be found in Zorec et al. (2009) and Aidelman et al. (2012).

Apart from the quantities derived from the BCD classification, we also refer to the apparent fundamental parameters as those used to represent spectra or whatever other observed quantity emitted in a given spectral range, most frequently in the visual spectral region, by rotationally deformed stellar atmospheres using classical plane-parallel model atmospheres

in radiative and hydrostatic equilibrium (Hubeny & Lanz 1995; Castelli & Kurucz 2003). The issued quantities ($T_{\rm eff}$, $\log g$) from the use of such model atmospheres are then called apparent fundamental parameters.

The method to determine apparent fundamental parameters based on the BCD (λ_1, D^*) parameters can be simply applied to B stars, both normal and peculiar, because the spectral characteristics due to the photosphere and circumstellar environments are located at different wavelengths. Thanks to this separation of spectral signatures of very different origins, it is obvious that for objects in which the radiation flux is strongly modified by the gaseous or dusty circumstellar material, like in Be and B[e] stars, the BCD system leads to a more reliable determination of ($T_{\rm eff}$, $\log g$, $M_{\rm V}$, $M_{\rm bol}$) than classic models of stellar atmospheres that cannot avoid the perturbation of line spectra or spectral energy distributions (SEDs) by the emissions and absorptions produced by extended envelopes (Cidale et al. 2001; Zorec et al. 2005). Up to now, the BCD classification system has not been systematically used for Bn stars. The measurement uncertainties affecting $T_{\rm eff}$, $M_{\rm V}$, and $M_{\rm bol}$ depend on the measurement errors made on the BCD quantities (λ_1, D^*), which on average produce $\Delta T_{\rm eff} \sim \pm 500$ K for the late B-type stars and ± 1500 K for the early B-types ($T_{\rm eff} > 20\,000$ K), $\Delta \log g \sim \pm 0.2$ dex, and $\Delta M \sim \pm 0.3$ mag both for $M_{\rm V}$ and $M_{\rm bol}$.

In some cases, rather significant deviations can be noted between determinations of $M_{\rm V}$ by different methods. Since it is frequently difficult to explain their origin, in this work we adopted for $M_{\rm V}$ the average of values estimated with the following different methods: the $M_{\rm V}(\lambda_1, D^*)$ BCD calibration, absolute magnitudes determined with the HIPPARCOS parallaxes (van Leeuwen 2007), and the calibration by Deutschman et al. (1976) of $M_{\rm V}$ as a function of MK spectral type, where the entry spectral type is the BCD spectral type/luminosity class. The $E(B-V)$ color excess that we employed to determine the absolute magnitude with parallaxes is also an average of several estimates determined through the BCD color gradient $\Phi_{\rm rb}$ (Aidelman et al. 2012; Gkouvelis et al. 2016), the color excess determined using the absorption depression at 2200 Å in the far-ultraviolet (far-UV) (Briot & Zorec 1987; Zorec & Briot 1991), the $(B-V)$ intrinsic colors given by Deutschman et al. (1976) as function of the spectral type, and the $E(B-V)$ derived from the interstellar absorption curve as a function of the distance in the direction of the studied objects (Neckel & Klare 1980).

Although the $M_{\rm V}$ derived from parallaxes can be a good determination of the absolute magnitude for stars in which the CE does not strongly mar the visible continuum energy distribution as in most Bn stars, it can, however, be affected by such flux excesses in Be stars with detectable CE spectral signatures (Ballereau et al. 1995; Moujtahid et al. 1998, 1999). In our Be star sample, this effect is expected to result in an uncertainty $\delta M_{\rm V} \simeq 0.1$ mag in the average $M_{\rm V}$. However, according to outbursts observed in Be stars, these magnitude changes can be as high as 0.3 mag (Hubert & Floquet 1998).

The bolometric absolute magnitude $M_{\rm bol}$ adopted in this work, from which we determine the apparent bolometric luminosity $L/L_\odot$ of stars, was calculated with

$$M_{\rm bol} = M_{\rm V} + {\rm BC}(T_{\rm eff}(\lambda_1, D^*)), \quad (3)$$

where BC($T_{\rm eff}$) is the bolometric correction applied by taking into account the warnings put forward by Torres (2010).

We had no high-resolution blue spectra to determine reliable $\log g$ parameters by fitting models of stellar atmospheres. This quantity is very uncertain since estimates based on models of stellar atmospheres and evolutionary tracks do not lead to the same value (Gerbaldi & Zorec 1993; Aidelman et al. 2012). Therefore, we adopted an indirect estimate using models of stellar evolution without rotation (Ekström et al. 2012) by interpolating in the evolutionary tracks the stellar $M/M_\odot$ as a function of $L/L_\odot$, determined as mentioned above, and the $T_{\rm eff}(\lambda_1, D^*)$.

In Tables A.3 and A.4 are reported the fundamental parameters derived as described above using the BCD spectrophotometric quantities together with other calibrations and methods. The $E(B-V)$ values are listed in Col. 6, while $M_{\rm V}$, $T_{\rm eff}$ and $\log L/L_\odot$, together with their uncertainties, are shown in Cols. 7–12. From the effective temperature $T_{\rm eff}(\lambda_1, D^*)$ and the bolometric luminosity $L/L_\odot$, we estimated another series of derived parameters using models of stellar evolution (Ekström et al. 2012). Tables A.5 and A.6 list these values for Be and Bn stars, respectively: stellar mass $M/M_\odot$ and its uncertainty are given in Cols. 2 and 3; values for $\log g$ and $\sigma_{\log g}$ are given in Cols. 4 and 5; the stellar radius $R/R_\odot$ and its uncertainty are given in Cols. 6–7; equatorial critical velocity $V_{\rm c}$, together with its uncertainties in Cols. 8 and 9; and the stellar age t in terms of the fractional age $t/t_{\rm MS}$, where $t_{\rm MS}$ is the time spent by a star of a given mass in the MS evolutionary phase, is given in Col. 10, and its uncertainties are listed in Col. 11.

For a quick overview of all these quantities, Fig. 9 gives a graphical presentation of observed (d, $V\sin i$, $V\sin i/V_{\rm c}$) and apparent fundamental parameters ($T_{\rm eff}$, $\log g$) through some relations between them. In this figure we note that B stars acquire their classification as Bn stars for apparent $V\sin i \gtrsim 50$ km s^{-1} (Fig. 9a) or $V\sin i/V_{\rm c} \gtrsim 0.4$ (Fig. 9b) and $T_{\rm eff} \lesssim 22\,500$ K (Figs. 9e,f). Also, the Bn stars in our sample have $\log g \gtrsim 3.8$, while Be stars may attain $\log g \sim 3.0$ (Figs. 9g,h).

In Fig. 10 we show the $T_{\rm eff}$ values against $V\sin i$ (a) and $V\sin i/V_{\rm c}$ (b), where the different symbols represent the appearance of the sBD for Be and Bn stars. Black squares indicate stars without a sBD, while orange triangles and green diamonds represent stars with the sBD in emission and absorption, respectively. It can be seen that the sBD in absorption appears for stars with $T_{\rm eff} \lesssim 22\,500$ and $V\sin i \gtrsim 250$ km s^{-1}, i.e., star-CE systems likely seen equator-on. On the other hand, the sBD in emission appears however likely for stars with $T_{\rm eff} \gtrsim 15\,000$ K and values of $V\sin i \lesssim 250$ km s^{-1}, which indicates that low inclination angles are privileged.

4.2. Relations between emission intensities and fundamental parameters

In Sect. 4.1 we determined the occurrence of the sBD as a function of $T_{\rm eff}$ and $V\sin i$ (or $V\sin i/V_{\rm c}$) for Be and Bn stars. We can go even a little further by searching for relations between the intensity of different emission (or absorption) signatures due to the CE and some fundamental parameters for Be stars. Since the formation regions of the emission in the Hα line and that of the sBD component are not the same, we expect to get information that may have an impact on the modeling of the physical structure of the CEs and perhaps of their formation process.

The amount of emission in the Hα line is presented in terms of its total equivalent width W in Å, where positive values of W correspond to emission lines and the flux $F_{\rm H\alpha}$ (erg cm^{-2} sec^{-1}). The total equivalent width is given as

$$W = W_{\rm e} + W_{\rm ph}, \quad (4)$$

where $W_{\rm e}$ represents the equivalent width of the emission superimposed to the underlying photospheric absorption line profile

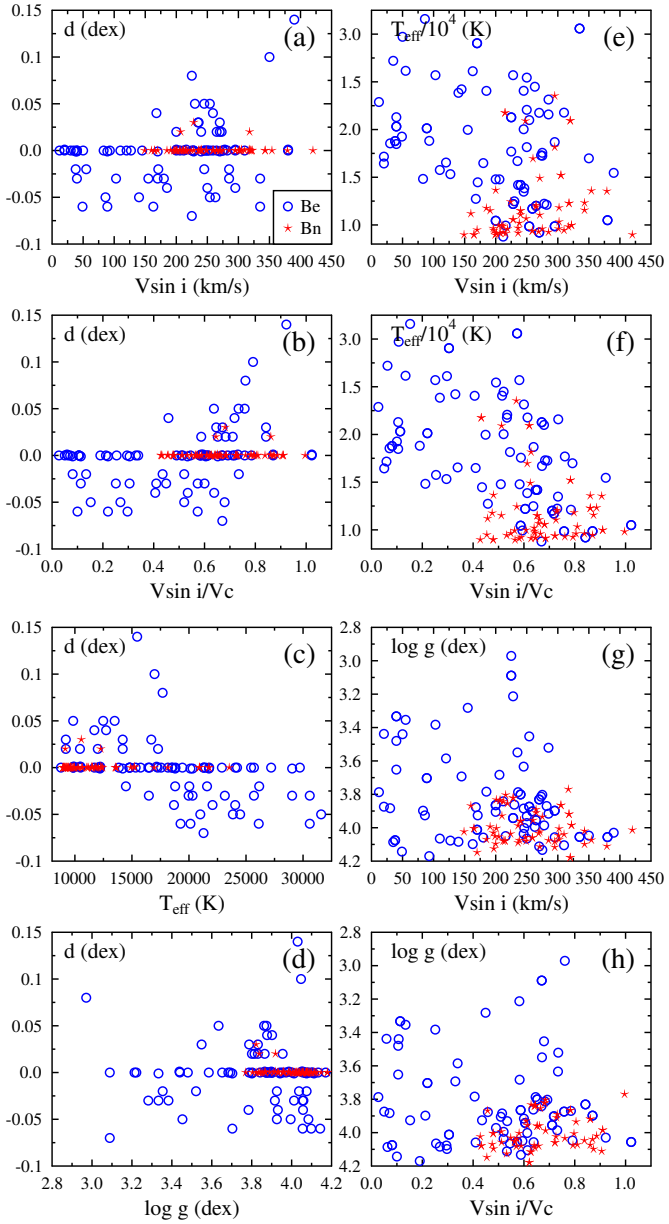

Fig. 9. Graphical presentation of observed ($d, V\sin i, V\sin i/V_c$) and apparent fundamental parameters ($T_{\rm eff}$, $\log g$) through some relations between these parameters. The blue empty circles represent Be stars, while the red stars represent Bn stars.

and $W_{\rm ph}$ is the equivalent width either of the total photospheric component or a fraction that was fitted with an empirical relation introduced by Ballereau et al. (1995), whose efficiency was since then proved by several authors (Chauville et al. 2001; Levenhagen & Leister 2006; Arias et al. 2018). The flux in the Hα line emission is calculated as $F_{\rm H\alpha} = W \times F^c_{\rm H\alpha}$, where $F^c_{\rm H\alpha}$ is the continuum flux at Hα line for the apparent ($T_{\rm eff}, \log g$) stellar parameters. In Table A.7 we present in turn values of W_e, W, $F_{\rm H\alpha}$, and d.

The results are shown in Fig. 11 where only tendencies are apparent but not tight correlations. A strong tendency is noted in Figs. 11a and b for enhanced sBD in emission ($d < 0$) as the emission in the Hα line increases, but the spread of points is very large, which indicates that probably different physical and geometrical structures and aspect angles of the CE can produce a given value of d (positive, negative, or even $d = 0$) for different amounts of emission in Hα line and vice versa. In

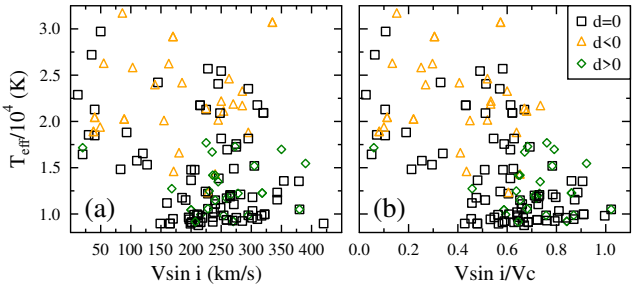

Fig. 10. Apparent $V\sin i$ (*panel a*) and $V\sin i/V_c$ (*panel b*) parameters for Be and Bn stars against $T_{\rm eff}$. Different symbols represent stars with $d < 0$ (orange triangles), $d > 0$ (green diamonds), and $d = 0$ (black squares).

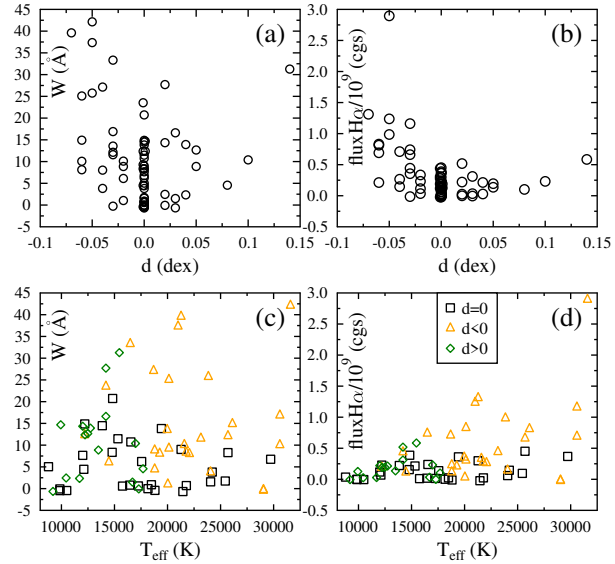

Fig. 11. *Panel a*: total equivalent widths in Å of the Hα line emission components for Be stars against the sBD component d in dex. *Panel b*: fluxes of the Hα line emission components against the sBD d in dex. *Panel c*: total equivalent widths in Å of the Hα line emission components against the apparent effective temperature. *Panel d*: fluxes of the Hα line emission components against the apparent effective temperature.

Fig. 11c we observe that Be stars without a sBD generally present small intensities in the Hα line over all the $T_{\rm eff}$ values. Also, for $T_{\rm eff} \gtrsim 15\,000$, where the sBD appears mostly in emission, the intensity of the Hα line become stronger as Teff increases. For $T_{\rm eff} \lesssim 17\,000$ and a sBD in absorption there is no clear effect of the effective temperature onto the strength of $d > 0$. For fluxes $0 \lesssim F_{\rm H\alpha}/10^9 \lesssim 0.5$ (erg cm^{-2} sec^{-1}), it is possible to have $d = 0$, but also all possible values of $d < 0$ or $d > 0$. Taking into account that early Be-type stars present a greater degree of variability (Labadie-Bartz et al. 2017), we expect to observe a wider range of Hα line intensity for higher $T_{\rm eff}$. Thus, the measurement of the intensity of the Hα line obtained from spectra taken at different dates than those of our low-resolution spectra may not represent the same state of the disk.

4.3. Parent nonrotating counterpart parameters

In what follows we study the properties of our program Be and Bn stars using stellar fundamental parameters corrected for rotational effects. The apparent fundamental parameters inferred directly from the observed spectra of stars are mainly functions

of the stellar mass $M/M_\odot$, fractional age $t/t_{\rm MS}$, inclination angle i of the rotation axis, and the law representing the angular velocity distribution inside and on the stellar surface $\Omega(r,\theta)$ corresponding to the current stellar evolutionary stage (r is the radial distance from the stellar center and θ is the co-latitude angle). This stellar angular velocity resumes the whole history of the angular momentum redistribution processes and the losses through the stellar mass-loss phenomena the star underwent since the zero age main sequence (ZAMS) and even before during the pre-MS phase. We do not have any information on the internal distribution of the stellar angular velocity. Therefore, to interpret the apparent rotation parameter $V\sin i$ at the current stellar evolutionary stage and the remaining fundamental parameters, we have to assume some rotation law. At the moment, our only option is to assume $\Omega(r,\theta)_{\rm surface} = \Omega_o$, i.e., Ω is uniform over the stellar surface (shellular rotation). In the present approach we also assume that Ω_o is a function of time, $\Omega_o = \Omega_o(t)$, and that it depends on the internal angular velocity evolution as described by the models calculated by Meynet & Maeder (2000), and Ekström et al. (2008, 2012). To take into account the effects of the rotation on the observed spectral characteristics, according to these models and assumptions, the following formal system of equations has to be solved in terms of the parameters $M/M_\odot$, $t/t_{\rm MS}$, $\Omega/\Omega_{\rm c}$ and i:

$$
\begin{aligned}
T_{\rm eff}^{\rm app} &= T_{\rm eff}^{\rm pnrc}(M,t)\, C_{\rm T}(M,t,\eta,i)\\
g_{\rm eff}^{\rm app} &= g_{\rm eff}^{\rm pnrc}(M,t)\, C_{\rm G}(M,t,\eta,i)\\
L^{\rm app} &= L^{\rm pnrc}(M,t)\, C_{\rm L}(M,t,\eta,i)\\
\frac{(V\sin i)_{\rm app}}{V_{\rm c}(M,t)} &= \left[\frac{\eta}{R_{\rm e}(M,t,\eta)/R_{\rm c}(M,t)}\right]^{1/2}\sin i - \frac{\Sigma(M,t,\eta,i)}{V_{\rm c}(M,t)},
\end{aligned}
\qquad (5)
$$

where $R_{\rm e}(M,t,\eta)$ and $R_{\rm c}(M,t)$ are the actual and the critical stellar equatorial radii corresponding to the current stellar evolutionary stage, respectively, which are determined using our 2D models of rigidly rotating stars (Zorec et al. 2011; Zorec & Royer 2012). The quantity $\eta = (\Omega/\Omega_{\rm c})^2[R_{\rm e}/R_{\rm c}]^3$ is the ratio of the centrifugal to the gravitational acceleration in the equator, and approaches 1 more slowly than $\Omega/\Omega_{\rm c}$ and $V/V_{\rm c}$ when the stellar rotation becomes critical. The left-hand side of Eq. (5) is associated with the apparent fundamental parameters determined in Sect. 4.1. On the right side of Eq. (5), $T_{\rm eff}^{\rm pnrc}(M,t)$, $g_{\rm eff}^{\rm pnrc}(M,t)$, $L^{\rm pnrc}(M,t)$ are the parent nonrotating counterpart (pnrc) parameters effective temperature, surface gravity, and bolometric luminosity (see definition of pnrc in Frémat et al. 2005). The functions $C_{\rm T}(M,t,\eta,i)$, $C_{\rm G}(M,t,\eta,i)$, and $C_{\rm L}(M,t,\eta,i)$ carry information relative to the change of parameters due to the geometrical deformation of the rotating star and of its GD over the observed hemisphere. Stoeckley's correction $\Sigma(\eta,i,M.t)$ of the $V\sin i$ parameter for GD depends on a power exponent β_1 of the effective temperature, which depends on the colatitude angle θ and the surface angular velocity ratio $\Omega/\Omega_{\rm c}$ (Zorec et al. 2016, 2017b). Since we do not master these dependencies, we take as an approximation $\beta_1 = 1$, which produces an overestimation of the GD effect. The method used to solve the system of Eqs. (5) is detailed in Zorec et al. (2016).

An entirely consistent determination of the pnrc parameters in Eq. (5) demands that the entry apparent quantities $(T_{\rm eff}, \log g_{\rm eff}, L/L_\odot)$ be independent. This was attempted by Zorec et al. (2016) for a sample of bright Be stars for which all the required observational material was available along with information on the photometric variation of the studied objects useful to correct the SEDs from the perturbations introduced by the CE. On the contrary, in the present case we do not have this information for all the program stars. However, to treat the entire sample in the same way we attempted to obtain a first order estimate of the rotational effects on the fundamental parameters by assuming that they are rapid rotators having the same surface angular velocity ratio $\Omega/\Omega_{\rm c} = 0.95$. The pnrc parameters are meant to represent the studied objects as they were without rotation. These are given in Tables A.8 and A.9 for Be and Bn stars, respectively. Columns 2–7 present $T_{\rm eff}$, $\sigma_{T_{\rm eff}}$, $\log L/L_\odot$, $\sigma_{\log L/L_\odot}$, $\log g$ and $\sigma_{\log g}$, Col. 8 gives $M/M_\odot$ with its uncertainties in Col. 9, $V\sin i$ and $V_{\rm c}$ with their uncertainties are presented in Cols. 10–13, while $t/t_{\rm MS}$ and $\sigma_{t/t_{\rm MS}}$ are given in Cols. 14 and 15.

5. Evolutionary status of Be and Bn stars

5.1. Hertzsprung–Russell diagram of our program stars

Since Be and Bn stars are both rapid rotators, we can ask whether they have similar structures or other common properties that would allow us to consider both of these stars as members of a single population and, in particular, to think of Bn stars as potential Be stars. We begin by comparing their evolutionary state by searching for possible signatures using the observed (apparent) parameters and those corrected for rotational effects. Figure 12a shows the HR diagram of the studied objects obtained with the apparent $(\log L/L_\odot, \log T_{\rm eff})$ parameters. Figure 12b shows the same HR diagram, but drawn with pairs $(\log L/L_\odot, \log T_{\rm eff})_{\Omega/\Omega_{\rm c}}$ calculated under the assumption of $\Omega/\Omega_{\rm c} = 0.95$. The evolutionary tracks are from Ekström et al. (2012) for $\Omega/\Omega_{\rm c} = 0$ in Fig. 12a and for $\Omega/\Omega_{\rm c} \neq 0$ in Fig. 12b, where the adopted equatorial linear velocity in the ZAMS is $V_o = 300$ km s^{-1}.

The main difference seen in the HR diagrams of Fig. 12 is that Bn stars have masses $M \lesssim 9\,M_\odot$, while Be stars range from $3\,M_\odot \lesssim M$ to $M \lesssim 20\,M_\odot$. The correction of bolometric luminosities and effective temperatures for rotation effects brings back the objects to younger evolutionary stages in the MS and transforms apparent blue supergiants into MS objects. Another characteristic that comes from the HR diagram is that our Bn stars are close to the ZAMS, while in the same mass interval ($4 \lesssim M/M_\odot \lesssim 9$) Be stars occupy the entire MS evolutionary span. Bn stars are more numerous than Be stars for masses $M/M_\odot \lesssim 4$, but both roughly share the same evolutionary domain.

5.2. Distribution of stellar ages in our sample

Another way to describe the evolutionary stage of the studied objects is using masses and ages determined from Eq. (5) with the help of evolutionary tracks without or with rotation as previously done in Zorec et al. (2005) and Martayan et al. (2007). From the inferred age ratios $t/t_{\rm MS}$ and masses $M/M_\odot$, we obtain the diagrams shown in Figs. 13a–d. In Figs. 13a and b the apparent parameters $(M/M_\odot, t/t_{\rm MS})$ are plotted without and with correction for rotation effects, respectively. Figures 13c and d depict zooms of Figs. 13a and b for masses $M/M_\odot < 10$, respectively, to better separate the behavior of Bn stars (red stars) from that of Be stars (blue points). The $(M/M_\odot, t/t_{\rm MS})$ diagrams suggest that Bn stars seem to fill up an apparent gap of Be stars nested in the mass range $2 \lesssim M/M_\odot \lesssim 4$, which encompasses a more or less large evolutionary span. The solution pairs $(M/M_\odot, t/t_{\rm MS})$ for our program objects locate both Be and Bn stars in the second half of the MS when rotational effects are not accounted for, while under the assumption of $\Omega/\Omega_{\rm c} = 0.95$ for all objects, the points for both type of stars scatter from the ZAMS to the terminal age main sequence (TAMS).

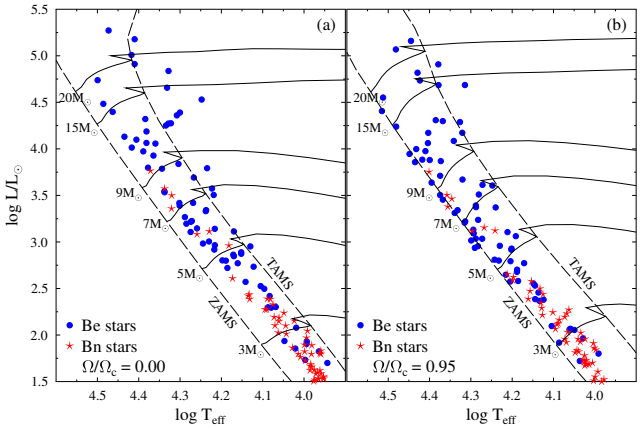

Fig. 12. *Panel a*: Hertzsprung-Russell (HR) diagram of the studied Be (blue points) and Bn stars (red stars) obtained with apparent ($\log L/L_\odot, \log T_{\rm eff}$) parameters (not treated for rotational effects). *Panel b*: HR diagram drawn with parameters corrected for rotational effects, assuming that all stars rotate at $\Omega/\Omega_{\rm c} = 0.95$. The evolutionary tracks are from Ekström et al. (2012) without rotation *a* and with rotation, with $V_o = 300$ km s^{-1} in the ZAMS *b*.

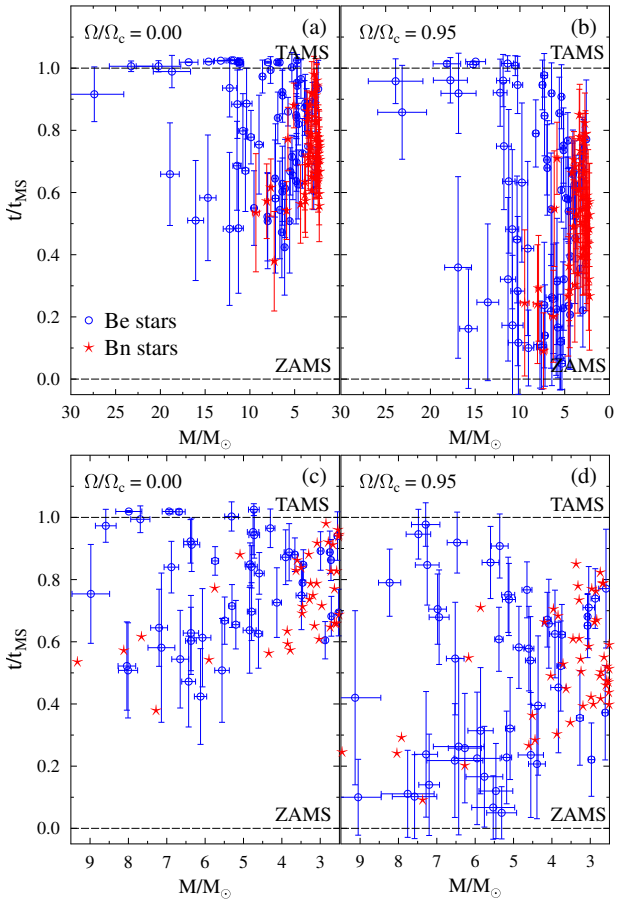

Fig. 13. Age vs. mass diagrams using the apparent pairs ($M/M_\odot, t/t_{\rm MS}$) not treated for rotation (*panels a and c*), and using parameters corrected for rotational effects (*panels b and d*). *Panels c and d*: zooms of *a* and *b* for masses $M/M_\odot < 10$, respectively. Error bars indicate uncertainties affecting the $t/t_{\rm MS}$ and $M/M_\odot$ determinations.

If Eq. (5) is solved assuming that the input parameters are entirely independent, we obtain a different estimate of $\Omega/\Omega_{\rm c}$ for each star. However, the new diagram ($M/M_\odot, t/t_{\rm MS}$) thus obtained does not differ strongly from Fig. 13. Nevertheless, even with the program star data available to us, it is impossible for us to derive a set of entirely independent input parameters ($T_{\rm eff}^{\rm app}, g_{\rm eff}^{\rm app}, L^{\rm app}, V\sin i_{\rm app}$). We can think of the group of three parameters $T_{\rm eff}^{\rm app}$, $g_{\rm eff}^{\rm app}$ (or $L_{\rm app}$), and $V\sin i_{\rm app}$ as independent, but $g_{\rm eff}^{\rm app}$ and $L_{\rm app}$ are mutually dependent because these parameters are obtained from $g_{\rm eff}^{\rm app} = g[T_{\rm eff}^{\rm app}, L_{\rm app}]$ or $L_{\rm app} = L_{\rm app}[T_{\rm eff}^{\rm app}, g_{\rm eff}^{\rm app}]$. For this reason, our results are only considered to be a first attempt to determine the evolutionary status of the program stars as rapid rotators.

In the mass interval $M/M_\odot \gtrsim 5$ it is likely that $(t/t_{\rm MS})_{\rm Bn} \lesssim (t/t_{\rm MS})_{\rm Be}$. In Fig. 13a, the higher values of $t/t_{\rm MS}$ ratios of Bn stars with $M/M_\odot \lesssim 4$ seem to suggest that they will never attain the required conditions to display the Be phenomenon during the MS evolutionary phase. Contrarily, in the diagrams where the parameters were corrected for rotational effects, we see that Bn stars can have age ratios $0.2 \lesssim (t/t_{\rm MS})_{\rm Bn} \lesssim 0.8$ if $M/M_\odot \lesssim 4$, whereas they have $0.0 \lesssim (t/t_{\rm MS})_{\rm Bn} \lesssim 0.2$ for masses $M/M_\odot \gtrsim 5$. According to Aidelman et al. (2018), the Be phenomenon is observed along the whole MS, and appears on average at an earlier age in massive stars than in the less massive stars. Thus, the possibility that the most massive Bn stars display the Be phenomenon at any time should not be excluded.

Regarding Bn stars, two questions can then be raised: first, do they have the required properties as rotators to display the Be phenomenon before they attain the TAMS? Second, are there CEs formed around these stars whose existence has not yet been detected because their temperatures are too low to excite emission lines?

6. Distribution of rotational velocities at the current stellar evolutionary stage

It is worth noting that there are selection effects marring the Be and Bn stellar sets employed in this work. On one hand, Be stars seen pole-on were somewhat privileged because they exhibit the most prominent sBD. On the other hand, Bn stars are currently identified as such when they are seen rather equator-on, otherwise the lack of emissions in their spectra do not enable us to identify those which rotate rapidly but are seen pole-on.

Figures 14a and b show the distributions of the observed (apparent) $V\sin i$ values of the program Be and Bn stars, respectively. In these figures, histograms correspond to the raw observed apparent velocity ratios $v = V\sin i/V_{\rm c}$. The superimposed green curves $\Psi(v)$ describe the smoothed distributions of the ratios $v = V\sin i/V_{\rm c}$ corrected for observational uncertainties. We preferred to use the ratios $V\sin i/V_{\rm c}$ instead of the $V\sin i$ parameters because the critical equatorial velocity $V_{\rm c}$ is estimated consistently with the mass and evolutionary state of each star, which then minimizes somewhat mass- and evolution-related effects on the distributions (Zorec et al. 2016). The class-steps of the histograms are established according to the bin-width optimization method by Shimazaki & Shinomoto (2007). The smoothed version of the frequency density distribution of ratios $v = V\sin i/V_{\rm c}$ corrected for measurement uncertainties were calculated using kernel estimators (Bowman & Azzalini 1997), where each observed parameter $v = V\sin i/V_{\rm c}$ is represented by a Gaussian distribution whose dispersion is given by the standard deviation of individual $V\sin i$ estimates.

In Fig. 14a we also added the distribution $\Psi(v)$ of ratios $v = V\sin i/V_{\rm c}$ corrected for observational uncertainties

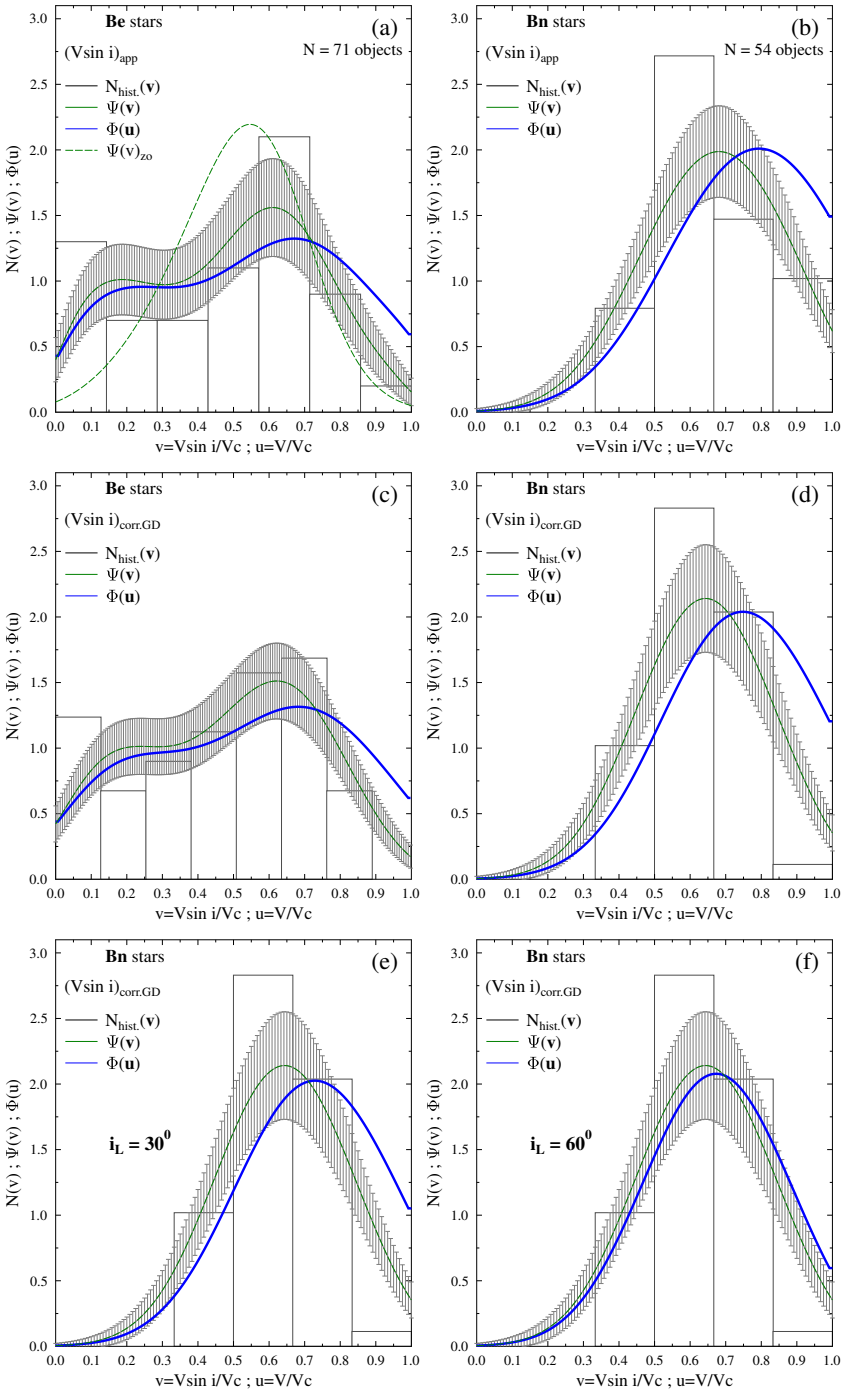

Fig. 14. Distributions without correction for GD effect. (*a*) Be and (*b*) Bn stars: histograms of apparent velocity ratios $v = V\sin i/V_c$; functions $\Psi(v)$ representing the smoothed histograms after correction for observational uncertainties (green curves); functions $\Phi(u)$ representing distributions of true velocity ratios $u = V/V_c$ (blue curves); in (*a*) $\Psi(v)$ from Zorec et al. (2016) (green dashed curve). Error bars in the smoothed histograms represent the statistical uncertainties that also concern the remaining distribution. (*c*) Be and (*d*) Bn stars: same as (*a*) and (*b*), but distributions of velocities corrected for GD effect. (*e*) and (*f*) histograms, functions $\Psi(v)$ from (*d*) and distributions of true velocity ratios $u = V/V_c$ for Bn star (blue curves), corrected for GD effect and for density probabilities of inclination angles restricted at inclinations $i_L = 30°$ and $i_L = 60°$, respectively.

determined in Zorec et al. (2016) for a sample nearly four times larger of Be stars than that used in this work. Comparing our $\Psi(v)$ and the same distribution for Be stars in Zorec et al. (2016) we note the effect carried by the bias affecting our Be sample, which privileges stars with as large as possible sBDs, and consequently does not warrant the random distribution of the inclination angles. Likewise, according to comments in Sect. 5.2, pole-on Bn stars are systematically missing in our sample, so that their distribution of apparent rotational velocity do not respect the randomness of inclination angles either. Nonetheless, we produced distributions of ratios of true velocities $u = V/V_c$ for both our Be and Bn stars as the inclination angles were distributed at random. We obtain thus the smoothed distributions $\Phi(u)$ shown in Figs. 14a–d (blue curves).

The lack of randomness of inclination angles in the distributions of Be rotational velocities presented in this work seems impossible to correct. We can, however, attempt to account for this lack in the distributions of Bn rotational velocities when transforming the distribution of ratios $v = V\sin i/V_c$ into $u = V/V_c$ ratios of true velocity ratios. To this end, we obliterate the probability density distribution of inclination angles from $i = 0°$ up to some limiting inclination i_L using a "guillotine[3]" function $G(i)$

[3] In this work, "guillotine" function means to obliterate the effectiveness of the probability function $P(i)$ in a given interval of inclination angles. We borrowed the term guillotine from the guillotine factor used to reduce Kramer's opacity in stellar interiors of low-mass stars (Eddington 1932).

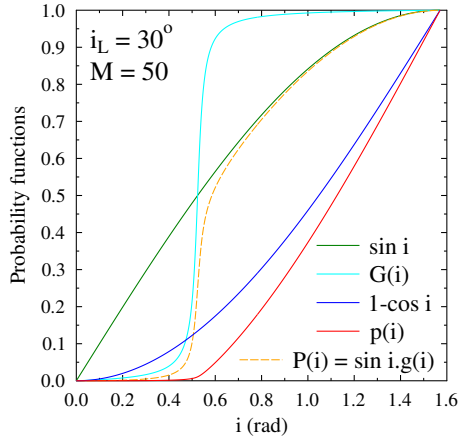

Fig. 15. Probability functions entering the definition of the guillotine function and obliterating the probability distribution of inclination angles.

as follows:

$$
\begin{aligned}
P(i)\,\mathrm{d}i &= \sin i.G(i)d\,i \\
G(i) &= A(M, i_{\rm L})\left[\frac{g(i) - g(0)}{g(\pi/2) - g(0)}\right] \\
g(i) &= \arctan[M(i - i_{\rm L})] \\
p(i) &= \int_0^i \sin i.G(i)\,\mathrm{d}i,
\end{aligned}
\tag{6}
$$

where $P(i)$ is normalized, i.e., $\int_0^{\pi/2} P(i)\,\mathrm{d}i = 1$, $A(M, i_{\rm L})$ is a normalization constant, and M is the "sharpness" of the cut. Figure 15 shows the behavior of functions entering the restrained probability function $p(i)$. Figures 14e and f show the distributions of ratios $u = V/V_{\rm c}$ of true velocities obtained by imposing $M = 50$, $i_{\rm L} = 30°$ and $i_{\rm L} = 60°$. All transformations of distributions of $v = V \sin i/V_{\rm c}$ into those of $u = V/V_{\rm c}$ are carried out in this work using the Richardson–Lucy deconvolution method (Richardson 1972; Lucy 1974). We note that increasing the value of M no sensitive effects are produced on the distribution functions obtained. The most outstanding results we can draw from Figs. 14c and d are that changing the value of $i_{\rm L}$ neither the skewness of the distribution is changed nor the mode (position of the maximum). The only characteristic that seems to vary a little more concerns the number of fastest stars: the higher the limiting inclination angle $i_{\rm L}$ the lower is the number of fast rotators, and accordingly the larger is the number of objects just behind the mode.

7. Distribution of Be and Bn star rotational velocities in the ZAMS

7.1. Inference of the $V/V_{\rm c}$ velocity ratios at the current stellar evolutionary stage

There is a final comparison we can make with velocity ratios $V/V_{\rm c}$ estimated for each star individually. This can be done using the system of Eqs. (5), where the angular velocity ratio $\Omega/\Omega_{\rm c}$, or the ratio $V/V_{\rm c}$ of linear rotational velocities are taken into account through the parameter $\eta = (\Omega/\Omega_{\rm c})^2(R_{\rm e}/R_{\rm c})^3 = (V/V_{\rm c})^2(R_{\rm e}/R_{\rm c})$. The solution of these equations can be drawn leaving the angular velocity ratio $\Omega/\Omega_{\rm c}$ as a free parameter, or by imposing a value for it. As already

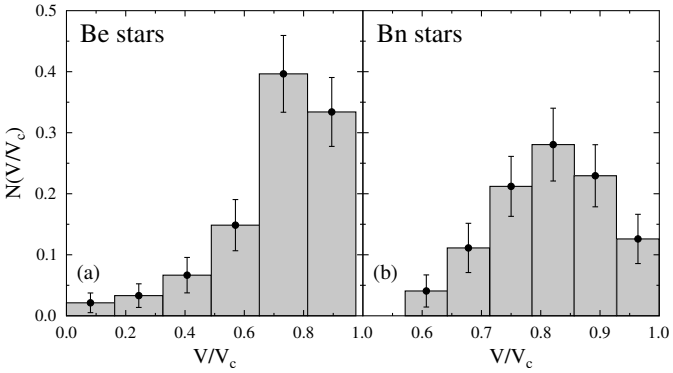

Fig. 16. Normalized histograms of true velocity ratios $V/V_{\rm c}$ at the current stellar evolutionary stage of Be (*panel a*) and Bn stars (*panel b*) obtained from Eq. (5).

commented in this paper, we have chosen the second possibility. The distribution of the $V/V_{\rm c}$ values is then necessarily different from that in Fig. 14 because no restriction is now imposed on the distribution of inclinations, while in Sect. 6 we assumed randomness or limiting it to the $(i_{\rm L}, \pi/2)$ interval. The results obtained for the ratios $V/V_{\rm c}$ at the current stellar evolutionary stage by solving Eq. (5) for $\Omega/\Omega_{\rm c} = 0.95$ are shown in Fig. 16 as normalized histograms. The outstanding differences between both distributions are: first, Bn stars seem to have ratios $V/V_{\rm c}$ that are strongly concentrated to the interval $0.6 \lesssim V/V_{\rm c} \lesssim 1.0$, which is the consequence of having missed pole-on Bn stars. Second, there are very few Be stars in our sample with $V/V_{\rm c} \lesssim 0.6$. Third, Be stars have a larger proportion of objects than Bn stars with ratios approaching 0.9–1.0. Fourth, the skewness of both distributions is likely negative, i.e., the mean and median are smaller than the mode. Fifth, the mode of distributions lies around $V/V_{\rm c} \sim 0.7$–0.8 for both types of objects.

7.2. Inference of $V/V_{\rm c}$ velocity ratios in the ZAMS

Model predictions of changes of the surface rotational velocity strongly depend on the prescribed mass-loss rate (Ekström et al. 2012). Mass loss is indeed a key phenomenon that controls the evolution of stars, so that high uncertainties may also affect the final results accordingly. For an initial look at the consequences from the evolution of rotational velocities as a consquence of the mass-loss phenomenon, it is interesting to use different prescriptions for the mass-loss rate for the whole sample of stars studied in this work (Be and Bn stars). Ekström et al. (2008) published two series of models for stars evolving with several initial rotational velocities and chemical compositions for the metallicity $Z = 0.02$. The first series of models depend on the mass-loss rates given by de Jager et al. (1988) and Kudritzki & Puls (2000), which in this work we call EMMB (Ekström et al. 2008); these rates are specified hereafter as $\dot{M}$(EMMB) mass-loss rates. The second series of models rely on the mass-loss rates suggested by Vink et al. (2000), which we call VdKL [VdKL = (Vink et al. 2000)], or $\dot{M}$(VdKL). These two mass-loss prescriptions differ somewhat at epoch $t/t_{\rm MS} \gtrsim 0.5$ and carry sensitive differences in the evolution of the $V/V_{\rm crit}$ velocity ratios by the end of the MS phase. These effects can be seen in Fig. 17 and affect stars with masses $M \gtrsim 9\ M_{\odot}$.

In each series of models we can adopt two different values to represent $V_{\rm ZAMS}$. There is the absolute initial $V_{\rm ZAMS}$ rotational velocity assigned to the models at the nominal $t/t_{\rm MS} = 0$. There is also the value attained by the star once the first phase

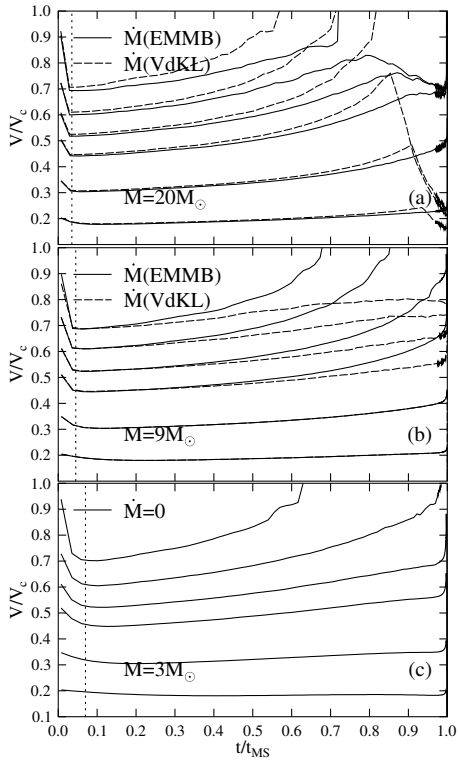

Fig. 17. Theoretical evolution of velocity ratios $V/V_{\rm crit}$ in the MS calculated by Ekström et al. (2008) with mass-loss rates $\dot{M}$(EMMB) (full lines) and $\dot{M}$(VdKL) (dashed lines) for $M = 3, 9$, and $20 M_{\odot}$. The vertical dotted lines near the ZAMS indicate the fractional age $t/t_{\rm MS}$ to which correspond the adopted ZAMS velocity ratios $V_{\rm ZAMS}/V_{\rm c}$.

of angular momentum redistribution occurs, which enables the object to acquire a stabilized rotational law. These phases last from 1 to 2% of the whole MS period, $t/t_{\rm MS} \sim 0.01-0.02$ (Meynet & Maeder 2000). We adopted the second value, because in real stars such a stabilization takes place in the pre-MS evolution, far before the stars cross the ZAMS to enter the long quasi-stationary MS phase.

The iteration of the system of Eqs. (5) with the use of the relations shown in Fig. 17 enables us to determine $V_{\rm ZAMS}$ of our program Be and Bn stars as a function of both mass-loss rates prescriptions, $\dot{M}$(EMMB) and $\dot{M}$(VdKL). The results obtained are presented in Fig. 18a for Be stars and Fig. 18b for Bn stars. We see that there is a tendency for a shift of points dependent on $\dot{M}$(EMMB) toward slightly lower $V_{\rm ZAMS}$ values than those calculated using models with $\dot{M}$(VdKL) mass-loss rates for stellar masses $M \lesssim 12 M_{\odot}$. The effect seems to be more marked among Be stars. The effect is less significant for Bn stars simply because the mass-loss rates are lower or zero for objects with masses $M \lesssim 4 M_{\odot}$ that concern most of our program Bn stars. Common average lower and upper limiting curves, $V_{\rm L}$ and $V_{\rm U}$, respectively, are represented in Figs. 18a and b. These limiting curves were determined by searching to include the highest possible number of stars inside the region. It is however interesting to note that although both type of objects begin their MS evolutionary phase with similar rotational velocities, only a fraction of these objects will at some moment display the Be phenomenon.

Another way of detecting possible differences in the ZAMS rotational velocity between Be and Bn stars and the effects carried by different prescriptions of mass-loss rates is shown in Fig. 19, where the histograms of ratios $(V/V_{\rm c})_{\rm ZAMS}$ are indicated. It is seen in this figure that for Be stars the values of $(V/V_{\rm c})_{\rm ZAMS}$ are slightly lower when the $\dot{M}$(VdKL) mass-loss rates are used, while differences are hardly noticeable for Bn stars. This is because only a few, the more massive Bn stars, undergo mass-loss phenomena. We also note that the skewness of the Be star distributions is negative, similar to what can be noted in Fig. 16 for the distribution of $V/V_{\rm c}$ corresponding to the current stellar evolutionary stage. Contrarily, the skewness of the Bn star distributions becomes positive (mean and median are larger than the mode), while it is likely negative in the respective distribution of $V/V_{\rm c}$ corresponding to the current stellar evolutionary stage shown in Fig. 16b.

We treat Eq. (5) by assuming that the input parameters are independent, therefore solutions of the $\Omega/\Omega_{\rm c}$ ratio are obtained for each star. In the case in which $\Omega/\Omega_{\rm c} = 0.95$ for all stars, the global aspect of the distribution of points is similar to Fig. 18 apart from punctual positions of points, and we do not show this. This is also true for the asymmetries of the distributions shown in Fig. 19. Owing to the number of uncertainties that mar our statistics, the results obtained must be taken just as indications for possibly differences or similarities between the Be and Bn star populations. Since they indicate that the distributions of rotational velocities could not be the same in the ZAMS, it would be interesting to carry out this type of study again with a higher number of objects, where all the parameters entering Eqs. (5) could be considered entirely independent. This would then enable us to establish the actual characteristic of distributions. If differences in their aspects could be confirmed, detailed studies carried out on the redistribution of internal angular momentum based on the derived initial distribution of rotational velocities would provide information to answer the question as to why some B-type rapid rotators in ZAMS cannot become Be.

8. Conclusions

In this paper we present observational characteristics of a sample of Be and Bn stars based on the behavior of their sBD, the Hα emission intensity, and their correlation with the stellar parameters (Sects. 2 and 3). Our Hα observations of the program Bn stars revealed that six stars previously considered in the literature as Bn stars, HD 31209, HD 42327, HD 43445, HD 165910, HD 171623, and HD 225132, are genuine Be stars. Since the rapid rotation characterizes both Be and Bn stars, the occasional appearance of some emission in the Hα Balmer line of Bn stars and the presence of signatures such as a sBD were motivating reasons to think that Bn and Be probably belong to the same class of objects.

We obtained low-resolution spectra in the visual region of the program stars and determined their (λ_1, D^*) parameters as defined in the BCD spectrophotometric stellar classification system. With these quantities, but also with the help of other methods and calibrations of stellar fundamental parameters, we determined the apparent fundamental parameters $(T_{\rm eff}, \log L/L_{\odot})$. Furthermore we measured the $V \sin i$ for a number of stars. Using the models of stellar evolution we also obtained their masses, radii, surface gravities, ages, and critical equatorial velocities $(M/M_{\odot}, R/R_{\odot}, \log g, t/t_{\rm MS}, V_{\rm c})$ (Sect. 4.1).

The correlations between the emission quantities and the apparent fundamental parameters gave us quantified tendencies, but these do not reveal tight correlations. Limits regarding effective temperatures and rotation velocities were found to characterize the appearance of the sBD in emission or in absorption (Sects. 4.1 and 4.2). A slightly more detailed statistical treatment

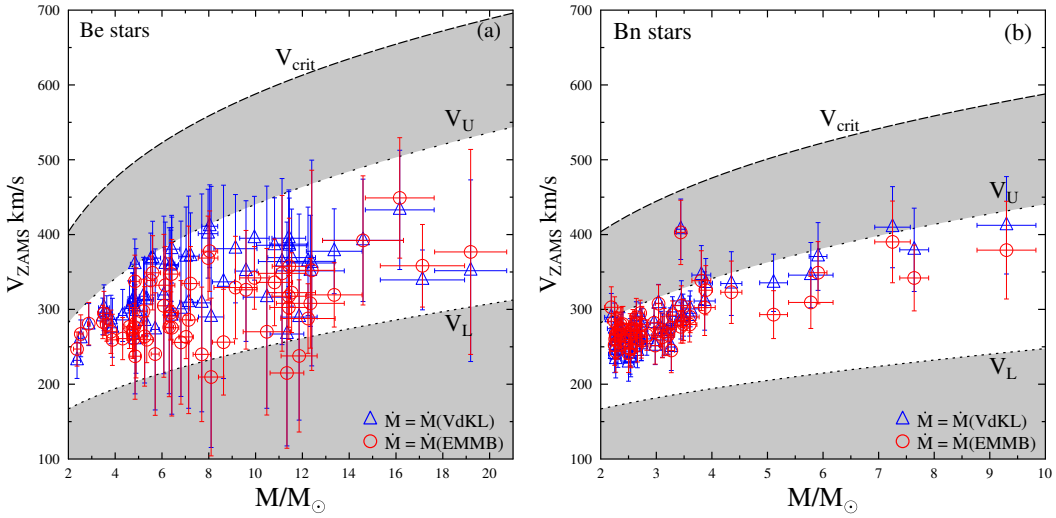

Fig. 18. Equatorial rotational velocities $V_{\rm ZAMS}$ of Be (*panel a*) and Bn (*panel b*) stars deduced using models of stellar evolution by Ekström et al. (2008) with mass-loss rates $\dot{M}$(EMMB) (red circles) and $\dot{M}$(VdKL) (blue triangles). In the figure is shown the curve $V_{\rm crit}$ in the ZAMS as a function of the stellar mass and the limiting curves $V_{\rm L}$ and $V_{\rm U}$ that surround the deduced $V_{\rm ZAMS}$ values.

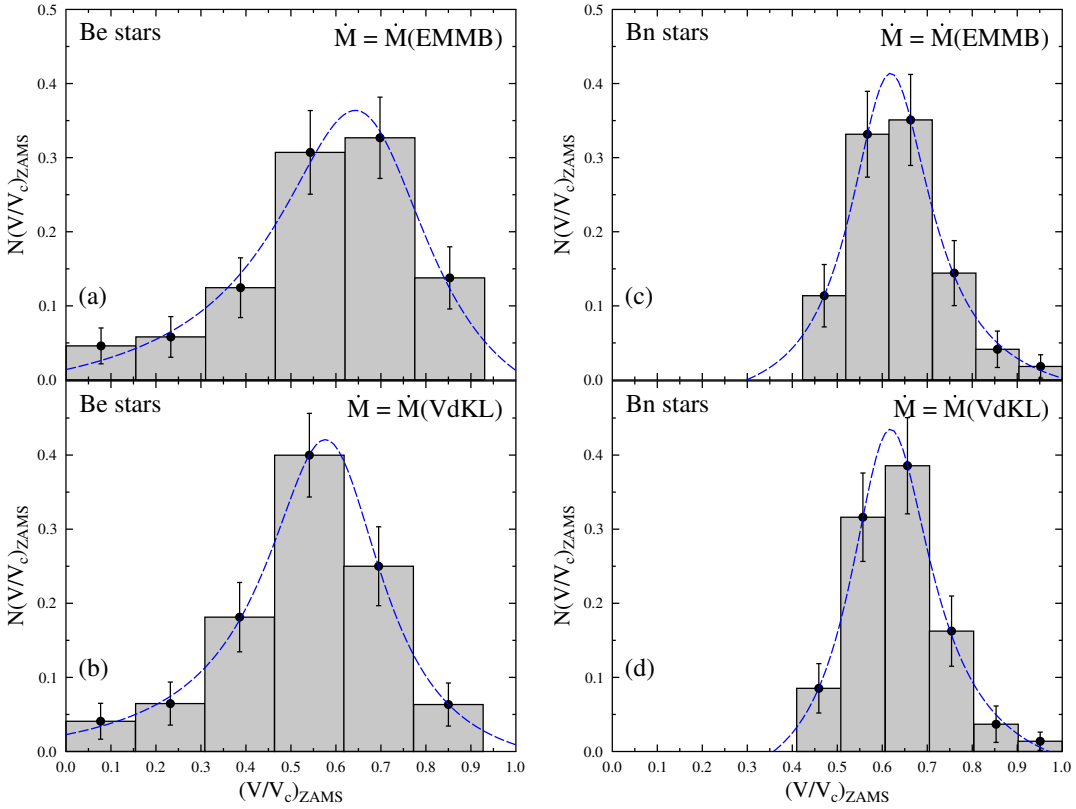

Fig. 19. Normalized histograms showing the distribution of ratios $V/V_{\rm c}$ in the ZAMS derived for the program Be (*panels a and b*) and Bn (*panels c and d*) stars. The results shown in *panels a and c* were obtained with EMMB mass-loss rates, while in *panels b and d* are for VdKL mass-loss rates. Error bars indicate sampling uncertainties according to the errors associated with the measured $V\sin i$ parameters. Fitted Person distributions are superimposed (blue dashed curves) to better perceive the differences in the asymmetries of distributions for each type of stars.

of the apparent $V\sin i$ parameters showed that the sBD in emission appear at angles lower than some 70°, while they appear in absorption at angles larger than some 60° (Sect. 3). This suggests that the CE layers close to the central star should have a large enough vertical height. In addition, we found than Be stars without a sBD generally present small intensities in the Hα line and that the intensity of the Hα line become stronger as $T_{\rm eff}$ increases when the sBD is in emission.

Because all the apparent fundamental parameters are not entirely independent, we estimated an order of magnitude of the correction we had to introduce for rotationally induced effects by assuming that all stars rotate at the angular velocity rate $\Omega/\Omega_{\rm c} = 0.95$ (Sect. 4.3). We could then place our program Be and Bn stars on an HR diagram and study their evolutionary status. We conclude that the main difference between Be and Bn stars is that Bn stars have masses $M \lesssim 9M_{\odot}$, while Be stars

range from $3M_\odot \lesssim M$ to $M \lesssim 20M_\odot$. We also note that Bn stars of masses $4 \lesssim M/M_\odot \lesssim 10$ are close to the ZAMS, while in this mass interval Be stars occupy the entire MS evolutionary span. Bn stars are more numerous than Be stars for masses $M/M_\odot \lesssim 4$, but both roughly share the same evolutionary domain (Sect. 5.1). From the study of the distribution of stellar ages we conclude that Bn stars can have age ratios $0.2 \lesssim (t/t_{\rm MS})_{\rm Bn} \lesssim 0.8$ if $M/M_\odot \lesssim 4$, whereas they have $0.0 \lesssim (t/t_{\rm MS})_{\rm Bn} \lesssim 0.2$ for masses are $M/M_\odot \gtrsim 5$ (Sect. 5.2). Thus, it should not be excluded that the most massive Bn stars could at any time display the Be phenomenon.

To characterize Be and Bn stars as fast rotators and thus find possible stellar population similarities or differences, we studied the distributions of true rotational velocity ratios $V/V_{\rm c}$ of our program stars at the current stellar evolutionary stage and in the ZAMS. We noted, in particular, biases that may be affecting the statistics due to selection effects concerning the aspect angles of the program stars. In spite of these difficulties, which we cannot overcome at the moment, initial indications seem to exist for differences in the velocity distributions. At the current stellar evolutionary stage, they have roughly the same global aspect (modes and negative skewness, as shown in Sect. 6), but their respective skewnesses do not have the same sign in the ZAMS; this sign is negative for Be stars and positive for Bn stars (Sect. 7). Studies similar to this work, but with more detail regarding the fundamental parameters and including a larger number of objects, might confirm our findings and succeed in deciding whether or not both type of objects are of the same class.

Finally, we comment on the disk structure near the central star that is suggested by some results of the present paper. Detailed accounts of successful representations of the observed emission in the Hα line of Be stars and of the continuum energy distribution from the far-UV to the IR, as well as of the polarization in the visible spectral range, are given in a series of rather recent papers and references therein (Araya et al. 2017; Arcos et al. 2017; Klement et al. 2017; Marr et al. 2018). In all these studies, the physical structure of the CE of Be stars is studied in the frame of an axisymmetric quasi-Keplerian disk in hydrostatic equilibrium in the vertical axis, where the scale height H is proportional to $R^{3/2}T^{1/2}$ and R represents the equatorial radius of the disk and T is its local temperature. However, from statistical arguments based on the study of the distribution of the $V \sin i$ parameter, we conclude in the present contribution that the sBD in emission could be seen in Be stars at inclination angles down to $i \sim 70°$, while this component should be in absorption in Be stars that have inclination angles $i \gtrsim 60°$. This finding may then conflict with the geometrically thin vertical structure of the density distribution of the above-mentioned flaring disks near the central star, where the sBD is raised. Thus, we could suggest an enlarged vertical scale height of the circumstellar disk near the central star. This idea is supported by the following results by different authors.

Simple models of circumstellar disks with electron densities above $N_{\rm e} = 10^{13}$ cm^{-3} near the central star can explain the increase of a sBD. However, at such gas densities, the sBD strongly encroaches the photospheric BD, which is rarely observed. To overcome the need for gas densities of disks near the star that are too high, a larger vertical scale of the disk than usually foreseen for pure Keplerian disks could then be envisioned. On the other hand, owing to the very rapid drop of the non-LTE source function of Fe II lines, two orders of magnitude within two stellar radii, Arias et al. (2006) and Zorec et al. (2007b), also suggested enlarged vertical scale heights. These zones are roughly the same where the sBD is formed. Also, larger vertical density scale heights can exist if the presence of possible disordered magnetic fields of low intensity is not neglected and if sources of heating energy in the disk near the central star are taken into account. In a series of papers, Kurfürst et al. (2018, and references therein) show that an equilibrium disk structure with enhanced density and a temperature increase up to some $T \sim 10^5$ K within 2 stellar radii is obtained through energy dissipation by viscosity. Such temperatures are able to increase the vertical scale heights of disks. Unfortunately, up to now there is neither observational evidence for such magnetic fields nor thorough hydro-dynamical calculations to confirm such dissipations in disks with enhanced vertical scale heights. Finally, we can ask whether smooth Keplerian density structures of disks near the star can survive when different types of mass ejections in Be stars takes place. In these objects continuous and variable winds with average rates $\dot{M} \sim 10^{-9}\ M_\odot\ {\rm yr}^{-1}$ (Snow 1981) can coexist together with discrete mass ejections of $\Delta M \lesssim 10^{-10}\ M_\odot$ (Guinan & Hayes 1984; Brown & Wood 1992; Hanuschik et al. 1993; Floquet et al. 2000; Hubert et al. 2000; Zorec et al. 2000). In such circumstances, the circumstellar environment may look very clumpy. The interaction of winds with the circumstellar clumps can build particular radial density structures (Arthur et al. 1994; Meilland et al. 2006) and produce shock fronts where $T_{\rm e} \gg T_{\rm eff}$ (Hartquist et al. 1986; Dyson & Hartquist 1992; Arthur et al. 1994).

These suggestions are speculations that may invite debate as well as requiring observational support and detailed hydrodynamical calculations to be accepted or rejected. It would then be advisable that in the future we proceed to model circumstellar disks with more physical requirements and try to model several spectral lines of different elements (Fe II emission lines, Hα, Hβ, Hγ to represent Balmer decrements, together with other IR emission lines) observed simultaneously, and other signatures of the disk, such as the sBD, which are sensitive to the up to now widely neglected physical inputs in circumstellar disks. Questions related to disk-wind interactions perhaps require observations made in the far-UV radiation, which at this time may seem unlikely.

Acknowledgements. We would like to thank Carol Jones, our referee, for her valuable comments and suggestions, which helped to improve our manuscript. This research has made use of the SIMBAD database, operated at CDS, Strasbourg, France. This work has made use of the BeSS database, operated at LESIA, Observatoire de Meudon, France: http://basebe.obspm.fr. We especially thank the following observers who have submitted data to BeSS that we have used in this publication: Christian Buil, Terry Bohlsen, André Favaro, Joan Guarro Fló, Bernard Heathcote and Nando Romeo. We thank also Christian Buil for his reduced individual Hα observations available via the spectroscopic Be-stars Atlas, http://www.astrosurf.com/buil/us/becat.htm. L.C. acknowledges financial support from CONICET (PIP 0177), the Agencia Nacional de Promoción Científica y Tecnológica (Préstamo BID PICT 2016-1971) and the Programa de Incentivos (G11/137) of the Universidad Nacional de La Plata (UNLP), Argentina. A.G. acknowledges the financial support received from the Agencia Nacional de Promoción Científica y Tecnológica of Argentina (PICT2017-3790).

References

Abt, H. A., Levato, H., & Grosso, M. 2002, ApJ, 573, 359
Adams, W. S., & Joy, A. H. 1923, ApJ, 57, 294
Aidelman, Y., Cidale, L. S., Zorec, J., & Arias, M. L. 2012, A&A, 544, A64
Aidelman, Y., Cidale, L. S., Zorec, J., & Panei, J. A. 2015, A&A, 577, A45
Aidelman, Y., Cidale, L. S., Zorec, J., & Panei, J. A. 2018, A&A, 610, A30
Araya, I., Jones, C. E., Curé, M., et al. 2017, ApJ, 846, 2
Arcos, C., Jones, C. E., Sigut, T. A. A., Kanaan, S., & Curé, M. 2017, ApJ, 842, 48
Arias, M. L., Zorec, J., Cidale, L., et al. 2006, A&A, 460, 821
Arias, M. L., Cidale, L. S., Kraus, M., et al. 2018, PASP, 130, 114201

Arthur, S. J., Dyson, J. E., & Hartquist, T. W. 1994, MNRAS, 269, 1117
Ballereau, D., Chauville, J., & Zorec, J. 1995, A&AS, 111, 423
Barbier, D., & Chalonge, D. 1939, ApJ, 90, 627
Barbier, D., & Chalonge, D. 1941, Ann. Astrophys., 4, 30
Barrera, L. H., Mennickent, R. E., & Vogt, N. 1991, Ap&SS, 185, 79
Bowman, A. W., & Azzalini, A. 1997, Applied Smoothing Techniques for Data Analysis: the Kernel Approach with S-plus Illustrations (Oxford, Uk: Oxford University Press)
Briot, D., & Zorec, J. 1987, IAU Colloq., 92, 214
Brown, A. G. A., & Verschueren, W. 1997, A&A, 319, 811
Brown, J. C., & Wood, K. 1992, A&A, 265, 663
Carciofi, A. C., & Bjorkman, J. E. 2008, ApJ, 684, 1374
Castelli, F., & Kurucz, R. L. 2003, IAU Symp., 210, A20
Chalonge, D., & Divan, L. 1952, Ann. Astrophys., 15, 201
Chauville, J., Zorec, J., Ballereau, D., et al. 2001, A&A, 378, 861
Cidale, L., Zorec, J., & Tringaniello, L. 2001, A&A, 368, 160
Cruzado, A., & Zorec, J. 2009, Boletin de la Asociacion Argentina de Astronomia La Plata Argentina, 52, 57
Dachs, J., Poetzel, R., & Kaiser, D. 1989, A&AS, 78, 487
de Jager, C., Nieuwenhuijzen, H., & van der Hucht, K. A. 1988, A&AS, 72, 259
Deutschman, W. A., Davis, R. J., & Schild, R. E. 1976, ApJS, 30, 97
Díaz, C. G., González, J. F., Levato, H., & Grosso, M. 2011, A&A, 531, A143
Divan, L. 1979, IAU Colloq., 9, 247
Divan, L., & Zorec, J. 1982, ESA SP, 177, 101
Divan, L., Zorec, J., & Briot, D. 1982, IAU Symp., 98, 53
Dworetsky, M. M. 1974, ApJS, 28, 101
Dyson, J. E., & Hartquist, T. W. 1992, Astrophys. Lett. Commun., 28, 301
Eddington, A. S., S. 1932, MNRAS, 92, 364
Ekström, S., Meynet, G., Maeder, A., & Barblan, F. 2008, A&A, 478, 467
Ekström, S., Georgy, C., Eggenberger, P., et al. 2012, A&A, 537, A146
Feinstein, A., & Marraco, H. G. 1979, AJ, 84, 1713
Floquet, M., Hubert, A. M., Hirata, R., et al. 2000, A&A, 362, 1020
Frémat, Y., Zorec, J., Hubert, A.-M., & Floquet, M. 2005, A&A, 440, 305
Gerbaldi, M., & Zorec, J. 1993, ASP Conf. Ser., 40, 150
Ghosh, K. K., Apparao, K. M. V., & Pukalenthi, S. 1999, A&AS, 134, 359
Gkouvelis, L., Fabregat, J., Zorec, J., et al. 2016, A&A, 591, A140
Guinan, E. F., & Hayes, D. P. 1984, ApJ, 287, L39
Hanuschik, R. W., Dachs, J., Baudzus, M., & Thimm, G. 1993, A&A, 274, 356
Hartquist, T. W., Dyson, J. E., Pettini, M., & Smith, L. J. 1986, MNRAS, 221, 715
Haubois, X., Carciofi, A. C., Rivinius, T., Okazaki, A. T., & Bjorkman, J. E. 2012, ApJ, 756, 156
Hirata, R., & Kogure, T. 1977, PASJ, 29, 477
Hoffleit, D., & Jaschek, C. 1982, The Bright Star Catalogue (New Haven, USA: Yale University Observatory)
Hubeny, I., & Lanz, T. 1995, ApJ, 439, 875
Hubert, A. M., & Floquet, M. 1998, A&A, 335, 565
Hubert, A. M., Floquet, M., & Zorec, J. 2000, ASP Conf. Ser., 214, 348
Hubert-Delplace, A.-M., & Hubert, H. 1979, An Atlas of Be Stars (Paris-Meudon Observatory)
Jaschek, C., & Jaschek, M. 1983, A&A, 117, 357
Jaschek, M., Slettebak, A., & Jaschek, C. 1981, Be Star Terminology, Be Star Newsletter
Kaiser, D. 1987, A&AS, 67, 203
Kaiser, D. 1989, A&A, 222, 187
Klement, R., Carciofi, A. C., Rivinius, T., et al. 2017, A&A, 601, A74
Kudritzki, R., & Puls, J. 2000, ARA&A, 38, 613
Kurfürst, P., Feldmeier, A., & Krtička, J. 2018, A&A, 613, A75
Labadie-Bartz, J., Pepper, J., McSwain, M. V., et al. 2017, AJ, 153, 252
Levenhagen, R. S., & Leister, N. V. 2006, MNRAS, 371, 252
Lucy, L. B. 1974, AJ, 79, 745
Marr, K. C., Jones, C. E., & Halonen, R. J. 2018, ApJ, 852, 103
Martayan, C., Frémat, Y., Hubert, A.-M., et al. 2007, A&A, 462, 683
Meilland, A., Stee, P., Zorec, J., & Kanaan, S. 2006, A&A, 455, 953
Mennickent, R. E., Sabogal, B., Granada, A., & Cidale, L. 2009, PASP, 121, 125
Meynet, G., & Maeder, A. 2000, A&A, 361, 101
Morgan, W. W., & Keenan, P. C. 1973, ARA&A, 11, 29
Moujtahid, A., Zorec, J., Hubert, A. M., Garcia, A., & Burki, G. 1998, A&AS, 129, 289
Moujtahid, A., Zorec, J., & Hubert, A. M. 1999, A&A, 349, 151
Moujtahid, A., Zorec, J., & Hubert, A. M. 2000, ASP Conf. Ser., 214, 510
Neckel, T., & Klare, G. 1980, A&AS, 42, 251
Neiner, C., de Batz, B., Cochard, F., et al. 2011, AJ, 142, 149
Peton, A. 1981, A&A, 101, 96
Poeckert, R., & Marlborough, J. M. 1978a, ApJ, 220, 940
Poeckert, R., & Marlborough, J. M. 1978b, ApJS, 38, 229
Porter, J. M., & Rivinius, T. 2003, PASP, 115, 1153
Richardson, W. H. 1972, J. Opt. Soc. Am., 62, 55
Rivinius, T., Štefl, S., & Baade, D. 2006, A&A, 459, 137
Rivinius, T., Carciofi, A. C., & Martayan, C. 2013, A&ARv, 21, 69
Sabogal, B. E., Ubaque, K. Y., García-Varela, A., Álvarez, M., & Salas, L. 2017, PASP, 129, 014203
Schild, R. E. 1978, ApJS, 37, 77
Shimazaki, H., & Shinomoto, S. 2007, Neural Comput., 19, 1503
Snow, T. P., Jr. 1981, ApJ, 251, 139
Slettebak, A. 1982, ApJS, 50, 55
Stoeckley, T. R. 1968, MNRAS, 140, 141
Strom, S. E., Wolff, S. C., & Dror, D. H. A. 2005, AJ, 129, 809
Torres, G. 2010, AJ, 140, 1158
Townsend, R. H. D., Owocki, S. P., & Howarth, I. D. 2004, MNRAS, 350, 189
Uesugi, A., & Fukuda, I. 1982, Catalogue of stellar rotational velocities (revised) (Kyoto: University of Kyoto, Departement of Astronomy)
Underhill, A., & Doazan, V. 1982, B Stars with and without Emission Lines, Parts 1 and 2 (Washington, DC: NASA)
van Leeuwen, F. 2007, A&A, 474, 653
Vieira, R. G., Carciofi, A. C., Bjorkman, J. E., et al. 2017, MNRAS, 464, 3071
Vink, J. S., de Koter, A., & Lamers, H. J. G. L. M. 2000, A&A, 362, 295
Wolff, S. C., Edwards, S., & Preston, G. W. 1982, ApJ, 252, 322
Yudin, R. V. 2001, A&A, 368, 912
Zorec, J. 1986, Thèse d'État: Structure et rotation differentielle dans le etoiles B avec et sans emission, Université Paris VII, Paris, France
Zorec, J. 2000, ASP Conf. Ser., 214, 51
Zorec, J., & Briot, D. 1991, A&A, 245, 150
Zorec, J., & Briot, D. 1997, A&A, 318, 443
Zorec, J., & Royer, F. 2012, A&A, 537, A120
Zorec, J., Frémat, Y., & Hubert, A. M. 2000, ASP Conf. Ser., 214, 330
Zorec, J., Frémat, Y., & Cidale, L. 2005, A&A, 441, 235
Zorec, J., Frémat, Y., Martayan, C., Cidale, L. S., & Torres, A. F. 2007a, ASP Conf. Ser., 361, A 539
Zorec, J., Arias, M. L., Cidale, L., & Ringuelet, A. E. 2007b, A&A, 470, 239
Zorec, J., Cidale, L., Arias, M. L., et al. 2009, A&A, 501, 297
Zorec, J., Frémat, Y., Domiciano de Souza, A., et al. 2011, A&A, 526, A87
Zorec, J., Frémat, Y., Domiciano de Souza, A., et al. 2016, A&A, 595, A132
Zorec, J., Frémat, Y., Domiciano de Souza, A., et al. 2017a, A&A, 602, A83
Zorec, J., Rieutord, M., Espinosa Lara, F., et al. 2017b, A&A, 606, A32

Appendix A: Tables

Table A.1. Observed Be stars.

HD	α	δ	V	Observation dates	
	(ICRS,J2000.0)	(ICRS,J2000.0)	[mag]	Low-resolution	High-resolution Hα
HD 10144	01:37:42.84548	−57:14:12.3101	0.46	03-09-04	03-09-10 [a]
HD 16582	02:39:28.95579	+00:19:42.6345	4.07	31-08-04	–
HD 23016	03:42:18.94710	+19:42:00.9206	5.69	31-08-04	07-09-02 [a]
HD 28248	04:24:06.90247	−57:15:11.3797	7.52	31-08-04	–
HD 28497	04:29:06.92534	−13:02:54.1234	5.41	31-08-04/11-02-14	11-12-06 [b]/10-02-14
HD 30076	04:44:05.32090	−08:30:12.8425	5.81	03-09-04/11-02-14	14-12-03 [b]/10-02-14
HD 30739	04:50:36.72298	+08:54:00.6493	4.35	02-09-04	11-12-16 [a]
HD 35165	05:21:16.86051	−34:20:42.1863	6.09	11-02-14	–
HD 35411	05:24:28.61672	−02:23:49.7311	3.35	02-09-04/12-11-16	14-10-07 [a]/29-11-16 [a]
HD 35468	05:25:07.86325	+06:20:58.9318	1.64	03-09-04/12-11-16	–
HD 36012	05:28:48.45661	+02:09:52.9672	7.24	31-08-04	01-11-01 [b]
HD 36861	05:35:08.277	+09:56:02.96	3.47	02-09-04	–
HD 37490	05:39:11.14632	+04:07:17.2795	4.59	02-09-04	01-11-04 [b]
HD 37971	05:41:41.51048	−16:43:32.9897	6.2	31-08-04	01-02-04 [a]
HD 44783	06:24:02.28361	+08:53:06.0389	6.22	03-09-04	03-11-06 [a]
HD 44996	06:24:20.57893	−12:57:42.9789	6.12	01-09-04/12-11-16	30-10-01 [b]/07-01-17 [a]
HD 45871	06:28:39.24252	−32:22:16.5985	5.74	11-02-14	09-02-14
HD 47054	06:36:35.33135	−05:12:40.1107	5.52	02-09-04/11-02-14	15-12-03 [b]/10-02-14
HD 49131	06:45:31.18914	−30:56:56.3342	5.52	01-09-04	14-02-09 [a]
HD 52089	06:58:37.54876	−28:58:19.5102	5.8	11-02-14	–
HD 56139	07:14:48.65387	−26:46:21.6097	1.5	01-09-04/11-02-14	20-11-04 [b] 10-02-14
HD 57150	07:18:18.39335	−36:44:02.2329	3.82	03-09-04	14-10-12 [a]
HD 58155	07:23:00.69779	−31:55:25.6090	3.82	12-02-14	10-02-14
HD 58343	07:24:40.18741	−16:12:05.3014	4.67	12-02-14	09-02-14
HD 60606	07:33:51.04374	−36:20:18.2110	5.43	12-02-14	09-02-14
HD 61224	07:37:38.80107	−14:26:26.7454	5.19	12-02-14	10-02-14
HD 65875	08:00:44.13428	−02:52:54.9140	5.44	12-02-14	08-02-14
HD 66194	07:58:50.55172	−60:49:28.0554	6.52	12-02-14	08-02-14
HD 71072	08:25:00.39591	−12:45:53.2340	6.59	12-02-14	08-02-14
HD 78764	09:05:38.37501	−70:32:18.5960	5.81	11-02-14	08-02-14
HD 86440	09:56:51.74167	−54:34:04.0390	6.85	11-02-14	–
HD 88825	10:13:01.14731	−59:55:05.1161	4.65	11-02-14	09-02-14
HD 89080	10:13:44.21739	−70:02:16.4563	3.45	11-02-14	09-02-14
HD 89884	10:21:59.40072	−18:02:04.1307	6.09	11-02-14	09-02-14
HD 90490	10:25:16.18597	−58:52:20.8524	3.33	11-02-14	09-02-14
HD 91120	10:30:59.83742	−13:35:18.4921	7.13	11-02-14	09-02-14
HD 91465	10:32:01.46297	−61:41:07.1963	7	11-02-14	08-02-14
HD 102776	11:49:41.06060	−63:47:18.5249	5.58	12-02-14	08-02-14
HD 124367	14:14:57.13838	−57:05:10.0544	5.07	03-09-04	10-05-17 [a]
HD 127449	14:33:36.77344	−58:49:14.8832	7.71	31-08-04	21-05-17 [a]
HD 131492	14:56:43.98738	−62:46:51.6579	5.11	03-09-04	02-05-15
HD 135734	15:18:32.02296	−47:52:30.9957	4.27	03-09-04	20-05-17
HD 137387	15:31:30.82178	−73:23:22.5291	5.49	02-09-04	22-07-12 [a]
HD 138769	15:35:53.24806	−44:57:30.1982	4.54	31-08-04	29-05-17 [a]
HD 142184	15:53:55.86404	−23:58:41.1522	5.4	02-09-04	31-05-03 [a]
HD 142983	15:58:11.36869	−14:16:45.6894	4.87	01-09-04	01-05-04 [b]
HD 148259	16:28:49.88611	−44:48:45.4048	7.42	31-08-04	30-07-12 [a]
HD 154243	17:05:52.8443	−36:35:17.473	8.05	31-08-04	–
HD 155436	17:13:43.7631	−44:43:45.215	9.33	03-09-04	09-09-12 [a]
HD 166182	18:08:45.49142	+20:48:52.4079	4.35	01-09-04	–
HD 166566	18:11:50.91317	−15:40:47.5071	7.99	02-09-04	24-07-09 [a]
HD 171054	18:33:08.6698	−13:54:43.464	9.14	03-09-04	–
HD 176304	18:59:17.34138	+10:08:27.6130	6.75	01-09-04	20-05-17
HD 178744	19:09:51.596	−00:25:41.21	6.32	01-09-04	–

Notes. All the spectra were obtained in CASLEO, with the exception of those denoted with [a]BeSS (Neiner et al. 2011) or [b]the Spectroscopic Be Stars Atlas (http://www.astrosurf.com/buil/us/becat.htm).

Table A.1. continued.

HD	α	δ	V	Observation dates	
	(ICRS,J2000.0)	(ICRS,J2000.0)	[mag]	Low-resolution	High-resolution Hα
HD 187567	19:50:17.47943	+07:54:08.6934	6.48	01-09-04	17-06-02 [b]
HD 187811	19:51:04.10821	+22:36:36.1732	4.96	03-09-04	18-05-04 [b]
HD 192044	20:12:00.70129	+26:28:43.7037	5.92	03-09-04	14-08-04 [b]
HD 193911	20:22:03.43042	+24:26:45.9574	5.56	01-09-04	27-05-04 [b]
HD 205637	21:37:04.83068	−19:27:57.6464	4.55	03-09-04	21-07-03 [b]
HD 208057	21:53:03.76826	+25:55:30.4902	5.08	01-09-04	23-07-03 [a]
HD 209014	22:00:50.22537	−28:27:13.4639	5.62	31-08-04/18-05-17	30-06-02 [b]/19-05-17
HD 209409	22:03:18.84403	−02:09:19.3067	4.69	03-09-04/18-05-17	21-07-03 [b]/19-05-17
HD 209522	22:04:36.76657	−26:49:20.4956	5.95	31-08-04	30-06-02 [b]
HD 210129	22:07:50.30397	+21:42:10.5319	5.78	31-08-04	22-07-03 [b]
HD 212076	23:03:52.61349	+03:49:12.1662	4.99	03-09-04	29-06-04 [b]
HD 217891	22:21:31.07511	+12:12:18.6628	4.52	03-09-04	30-11-04 [a]
HD 256577	06:24:00.17698	+08:18:02.4935	9.77	01-09-04	25-01-03 [a]

Table A.2. Observed Bn stars.

HD	α	δ	V	Observation dates	
	(ICRS,J2000.0)	(ICRS,J2000.0)	[mag]	Low-resolution	High-resolution
HD 560	00:10:02.20293	+11:08:44.9280	5.53	31-08-04	–
HD 5617	00:57:37.76060	−18:59:55.0309	6.9	31-08-04	–
HD 10161	01:38:49.99449	−25:01:19.9155	6.69	31-08-04	–
HD 10894	01:47:09.10651	+10:50:39.2638	7.05	31-08-04	–
HD 15130	02:25:57.00560	−12:17:25.7104	4.87	31-08-04	–
HD 18331	02:56:37.42306	−03:42:44.3505	5.16	01-09-04	–
HD 18546	02:57:32.62737	−38:11:27.3204	6.41	01-09-04	–
HD 21364	03:27:10.15071	+09:43:57.6343	3.75	01-09-04	–
HD 24817	03:57:01.71819	+06:02:23.8921	6.07	01-09-04	–
HD 26676	04:13:34.56718	+10:12:44.8447	6.25	01-09-04	–
HD 26793	04:14:36.23274	+10:00:41.0529	5.22	02-09-04/11-11-16	13-11-16
HD 31093	04:51:28.21644	−34:54:22.6341	5.83	02-09-04	–
HD 31209	04:53:55.80621	+01:34:09.7362	6.61	02-09-04/12-11-16	13-11-16
HD 32039	05:00:32.52965	+03:36:53.3018	7.02	01-09-04	–
HD 32040	05:00:33.93059	+03:36:56.6825	6.63	01-09-04	–
HD 32309	05:01:25.58052	−20:03:06.9147	4.88	03-09-04	–
HD 34748	05:19:35.28351	−01:24:42.8149	6.35	03-09-04	–
HD 34863	05:19:59.02275	−12:18:56.1139	5.28	02-09-04	–
HD 35407	05:24:36.10074	+02:21:11.3943	6.3	03-09-04	–
HD 35640	05:26:02.36312	−05:31:06.6127	6.23	02-09-04	–
HD 35656	05:26:38.82954	+06:52:07.1619	6.4	02-09-04	–
HD 36058	05:28:56.90949	−03:18:26.7444	6.38	02-09-04	–
HD 42327	06:09:20.19816	−18:07:34.9889	6.36	03-09-04/12-11-16	14-11-16
HD 43445	06:15:44.88569	−13:43:06.2928	5	03-09-04/11-11-16	14-11-16
HD 45380	06:26:44.85077	−07:30:43.0061	6.33	02-09-04	–
HD 145122	16:08:46.63073	+17:12:20.2866	6.13	03-09-04/18-05-17	19-05-17
HD 149485	16:38:52.70554	−60:59:25.4506	6.15	03-09-04	–
HD 158094	17:31:05.91272	−60:41:01.8522	3.62	02-09-04	–
HD 159358	17:34:46.35143	−11:14:31.1929	5.54	03-09-04/18-05-17	20-05-17
HD 160181	17:37:31.09487	+24:18:35.9668	5.76	03-09-04/18-05-17	20-05-17
HD 164577	18:01:45.19884	+01:18:18.2775	4.43	02-09-04	–
HD 164900	18:02:30.15394	+22:55:23.6186	6.21	03-09-04	–
HD 165910	18:07:47.987	+13:04:15.27	6.6	03-09-04/18-05-17	19-05-17
HD 168905	18:24:18.24063	−44:06:36.9181	5.23	02-09-04	–
HD 171149	18:33:22.70821	−05:54:42.1805	6.35	02-09-04	–
HD 171623	18:35:12.60300	+18:12:12.2800	5.79	03-09-04/18-05-17	20-05-17
HD 172777	18:43:46.94185	−38:19:24.3885	5.11	02-09-04	–
HD 177724	19:05:24.60802	+13:51:48.5182	2.99	02-09-04	–

Notes. All the spectra were obtained in CASLEO.

Table A.2. continued.

HD	α	δ	V	Observation dates	
	(ICRS,J2000.0)	(ICRS,J2000.0)	[mag]	Low-resolution	High-resolution
HD 177756	19:06:14.93898	−04:52:57.2007	3.43	01-09-04	–
HD 179648	19:12:36.73270	+21:33:16.4573	6.04	03-09-04/18-05-17	19-05-17
HD 180183	19:18:41.54336	−56:08:40.8907	6.82	02-09-04/18-05-17	19-05-17
HD 180782	19:17:48.18680	+02:01:54.2136	6.17	01-09-04	–
HD 181296	19:22:51.20620	−54:25:26.1473	5.02	02-09-04	–
HD 182180	19:24:30.18046	−27:51:57.3957	6.01	02-09-04/18-05-17	19-05-17
HD 182645	19:26:11.04276	−15:03:11.7021	5.71	01-09-04/18-05-17	19-05-17
HD 183537	19:29:20.89711	+20:16:47.0613	6.33	03-09-04/18-05-17	19-05-17
HD 184606	19:34:34.89569	+19:46:24.2462	5	02-09-04	–
HD 188293	19:54:37.65152	−08:13:38.2390	5.71	01-09-04	–
HD 190454	20:05:26.33497	−12:39:54.5908	6.53	02-09-04	–
HD 195922	20:33:53.70161	+10:03:35.0469	6.54	02-09-04	–
HD 198529	20:51:58.76157	−33:10:40.7037	6.05	02-09-04	–
HD 199280	20:56:18.25465	−03:33:42.0926	6.56	01-09-04	–
HD 208321	21:56:22.76964	−37:15:13.1601	5.44	01-09-04	–
HD 210419	22:10:21.10793	−03:53:38.7132	6.28	01-09-04/11-11-16	14-11-16
HD 213998	22:35:21.38126	−00:07:02.9888	4.03	31-08-04	–
HD 215143	22:43:14.26259	−06:57:46.5799	6.41	01-09-04	–
HD 218639	23:09:49.54971	−14:30:37.9818	6.43	01-09-04	–
HD 219659	23:17:40.08278	−11:42:46.5910	6.33	01-09-04	–
HD 222847	23:44:12.07893	−18:16:36.9688	5.24	31-08-04	–
HD 223785	23:52:39.88172	−18:33:42.7496	6.82	02-09-04	–
HD 225132	00:03:44.38784	−17:20:09.5719	4.54	31-08-04/11-11-16	14-11-16

Table A.3. Observed BCD and apparent parameters of Be stars.

HD	D_* [dex]	λ_1 [Å]	SpTLC	d [dex]	$E(B-V)$ [mag]	M_V [mag]	σ_{M_V} [mag]	$T_{\rm eff}$ [K]	$\sigma_{T_{\rm eff}}$ [K]	$\log L/L_\odot$ [dex]	$\sigma_{\log L/L_\odot}$ [dex]	$V\sin i$ [km s^{-1}]	$\sigma_{V\sin i}$ [km s^{-1}]	Ref.
HD 10144	0.22	37	B4-5III	0.03	0.02	−2.68	0.17	16 697	1119	3.574	0.060	235	28	1
HD 16582	0.14	49	B2III	0.00	0.02	−3.11	0.46	22 885	1888	4.057	0.129	12	1	2
HD 23016	0.38	48	B8IV	0.00	0.10	−0.52	0.22	12 111	257	2.419	0.057	282	33	3
HD 28248	0.13	49	B2III	0.00	0.18	−3.46	0.15	20 000	2000	3.390	0.055	30	3	3
HD 28497	0.09	65	B0.5V	−0.03/−0.06	0.04	−3.42	0.39	30 588	1912	4.484	0.108	335	40	1
HD 30076	0.11	37	B2II	−0.07/0.00	0.09	−5.24	0.37	21 278	2202	4.837	0.114	225	27	4
HD 30739	0.54	64	A1-2IV	0.00	0.01	0.71	0.56	8781	349	1.700	0.143	212	25	3
HD 31209	0.53	58	A1IV	0.02/0.03	0.04	0.46	0.44	9204	251	1.824	0.112	270	32	3
HD 35165	0.24	54	B4V	0.10	0.02	−1.21	0.15	16 982	573	3.005	0.044	350	42	2
HD 35411	0.10	72	B1VI	em/−0.03	0.08	−3.35	0.49	29 043	2138	4.397	0.133	170	20	1
HD 35468	0.14	39	B2II-III	em/−0.03	0.02	−4.16	0.24	20 316	1800	4.360	0.082	40	4	2
HD 36012	0.25	54	B4V	−0.03	0.10	−1.07	0.20	16 484	516	2.918	0.054	180	21	2
HD 36861	0.06	42	B0.5Ib	−0.02	0.11	−5.15	0.85	26 156	1969	5.009	0.221	55	6	2
HD 37490	0.14	38	B2II	−0.03	0.11	−4.28	0.44	19 968	1833	4.390	0.127	155	18	5
HD 37971	0.25	46	B5IV	0.00	0.04	−1.63	0.14	16 441	537	3.141	0.042	20	2	6
HD 42327	0.45	62	B9.5V	abs/0.00	0.00	0.61	0.23	10 498	288	1.855	0.059	380	45	3
HD 43445	0.40	51	B8-9IV	0.00/0.04	0.01	−0.30	0.23	11 705	273	2.301	0.061	259	31	3
HD 44783	0.36	48	B7IV	0.05	0.03	−0.65	0.48	12 481	481	2.497	0.124	230	27	7
HD 44996	0.21	56	B3-4V	em/−0.02	0.09	−1.50	0.05	18 788	834	3.217	0.031	38	4	2
HD 45871	0.23	67	B4-5V	0.00	0.02	−1.08	0.35	17 561	849	2.983	0.095	275	33	2
HD 47054	0.38	55	B8V	0.00/em	0.04	−0.33	0.17	12 199	414	2.335	0.048	228	27	3
HD 49131	0.14	54	B2IV	0.00	0.04	−3.00	0.27	24 062	1736	4.064	0.082	245	29	2
HD 52089	0.12	66	B1.5V	0.00	0.03	−2.85	0.28	27 203	2267	4.131	0.089	35	4	10
HD 56139	0.18	46	B3III	−0.06/em	0.03	−2.88	0.31	20 129	959	3.838	0.085	89	10	4
HD 57150	0.14	41	B2III	−0.05	0.07	−3.87	0.27	20 993	1933	4.275	0.089	254	30	8
HD 58155	0.22	60	B4V	0.00	0.03	−1.40	0.38	18 157	1025	3.146	0.103	250	30	9
HD 58343	0.20	77	B4-5VI	−0.06	0.17	−1.38	0.29	19 261	755	3.196	0.078	49	5	4
HD 60606	0.14	43	B2III	−0.02	0.08	−3.74	0.20	21 584	1937	4.251	0.076	285	34	4
HD 61224	0.29	41	B6III	0.00	0.11	−1.82	0.26	14 781	918	3.113	0.075	206	24	3

References. $V\sin i$ values taken from: (1) Zorec et al. (2005); (2) Levenhagen & Leister (2006); (3) Zorec & Royer (2012); (4) Frémat et al. (2005); (5) Chauville et al. (2001); (6) Wolff et al. (1982); (7) Abt et al. (2002); (8) Yudin (2001); (9) Slettebak (1982); (10) Uesugi & Fukuda (1982); (11) this work.

Table A.3. continued.

HD	D_* [dex]	λ_1 [Å]	SpTLC	d [dex]	$E(B-V)$ [mag]	M_V [mag]	σ_{M_V} [mag]	$T_{\rm eff}$ [K]	$\sigma_{T_{\rm eff}}$ [K]	$\log L/L_\odot$ [dex]	$\sigma_{\log L/L_\odot}$ [dex]	$V\sin i$ [km s^{-1}]	$\sigma_{V\sin i}$ [km s^{-1}]	Ref.
HD 65875	0.12	81	B2IV	−0.06	0.12	−2.67	0.58	26 116	1240	4.014	0.150	163	19	4
HD 66194	0.15	48	B2III	−0.04	0.10	−2.52	0.54	22 065	1631	3.787	0.145	250	30	10
HD 71072	0.23	47	B4IV	0.02	0.07	−1.99	0.23	17 290	1022	3.331	0.068	273	32	1
HD 78764	0.12	49	B2III	0.00	0.07	−3.63	0.52	24 215	2042	4.321	0.143	145	17	10
HD 86440	0.20	36	B4III	abs	0.11	−3.16	0.31	17 161	1606	3.792	0.098	20	2	10
HD 88825	0.23	38	B4-5III	0.00	0.10	−2.53	0.13	16 542	1125	3.505	0.053	120	3	11
HD 89080	0.33	39	B7III	0.05	0.05	−1.62	0.25	13 485	820	2.952	0.073	245	29	4
HD 89884	0.29	71	B7VI	0.00	0.02	−0.61	0.30	13 851	803	2.571	0.082	246	44	1
HD 90490	0.27	58	B5V	0.00	0.08	−0.75	0.24	15 326	680	2.721	0.066	127	44	1
HD 91120	0.47	68	A0-1V	abs	0.05	0.81	0.29	9935	319	1.733	0.076	216	25	1
HD 91465	0.15	54	B2IV	−0.03	0.10	−2.76	0.32	23 143	1083	3.928	0.087	285	34	4
HD 102776	0.17	64	B2.5V	em	0.05	−1.93	0.25	21 754	1021	3.534	0.069	270	32	10
HD 124367	0.21	52	B3-4IV-V	−0.04	0.09	−1.53	0.36	18 686	736	3.225	0.096	295	35	1
HD 127449	0.20	55	B3V	0.00	0.15	−1.54	0.33	19 423	951	3.267	0.089	–	–	1
HD 131492	0.13	51	B2III-IV	−0.04	0.15	−3.31	0.38	24 053	1908	4.187	0.108	185	22	1
HD 135734	0.36	60	B8V	abs	0.03	−0.20	0.50	12 225	539	2.298	0.129	278	33	1
HD 137387	0.13	55	B2IV	0.00	0.13	−2.95	0.17	25 444	1840	4.099	0.063	250	30	1
HD 138769	0.21	64	B4V	0.00	0.03	−1.22	0.18	18 813	841	3.107	0.054	93	11	8
HD 142184	0.17	60	B2.5V	0.00	0.17	−1.95	0.13	21 774	1051	3.544	0.045	310	37	1
HD 142983	0.27	55	B5V	0.14	0.09	−0.93	0.24	15 459	668	2.799	0.066	390	46	1
HD 148259	0.08	57	B0.5IV	−0.05	0.47	−3.97	0.00	31 586	2849	4.738	0.065	86	10	8
HD 154243	0.14	56	B2IV-V	−0.05	0.34	−2.73	0.10	24 487	1557	3.973	0.048	263	1	1
HD 155436	0.07	43	B0.5Ib-II	0.00	1.04	−5.62	0.53	25 696	3187	5.178	0.157	228	3	1
HD 165910	0.50	55	A0IV	0.05/0.00	0.07	0.30	0.29	9850	259	1.932	0.075	254	30	3
HD 166182	0.21	49	B3-4IV	0.00	0.07	−2.04	0.25	18 551	941	3.420	0.071	30	3	7
HD 166566	0.06	46	B0II	0.00	0.39	−5.48	0.51	29 720	4048	5.272	0.159	50	6	2
HD 171054	0.14	42	B2III	0.00	0.40	−3.83	0.21	21 293	1915	4.272	0.078	40	4	2
HD 171623	0.50	54	A0IV	abs/0.00	0.03	0.37	0.27	9861	291	1.905	0.070	295	35	10
HD 176304	0.20	43	B3-4III	0.00	0.41	−2.73	0.18	18 482	1294	3.692	0.064	40	4	7
HD 178744	0.29	49	B5-6IV	0.00	0.10	−1.15	0.41	14 784	388	2.847	0.104	200	24	7
HD 187567	0.15	64	B2V	−0.05	0.17	−2.35	0.29	23 848	787	3.798	0.078	140	16	7
HD 187811	0.19	54	B3IV-V	−0.02	0.05	−1.84	0.25	20 029	1017	3.419	0.071	245	29	1
HD 192044	0.31	43	B6III-IV	0.03	0.04	−1.35	0.26	14 191	733	2.889	0.072	236	28	3
HD 193911	0.35	50	B7V	0.04	0.06	−0.68	0.45	12 736	472	2.526	0.116	168	20	4
HD 205637	0.15	31	B3-4Ib-II	0.08	0.02	−4.93	0.35	17 691	1896	4.530	0.111	225	27	1
HD 208057	0.26	61	B5V	0.00	0.03	−0.89	0.44	15 759	711	2.802	0.116	110	13	4
HD 209014	0.38	54	B8IV-V	0.02/0.00	0.04	−0.23	0.20	12 007	466	2.294	0.054	265	31	3
HD 209409	0.31	43	B6IV-V	0.02/em	0.04	−1.31	0.28	14 191	667	2.873	0.076	240	28	3
HD 209522	0.23	46	B4III-IV	0.00	0.03	−2.02	0.28	17 255	691	3.342	0.076	275	33	1
HD 210129	0.30	48	B5IV	−0.02	0.09	−1.01	0.33	14 471	497	2.771	0.085	171	20	3
HD 212076	0.07	43	B0.5Ib-II	−0.03	0.12	−4.96	0.73	25 696	3584	4.911	0.207	103	12	4
HD 217891	0.29	47	B5-6IV	0.00	0.04	−1.18	0.32	14 827	544	2.863	0.083	83	9	3
HD 225132	0.47	50	B9.5IV	0.02/abs	0.01	0.04	0.16	10 444	274	2.079	0.042	200	24	7
HD 256577	0.12	39	B2II	0.00	0.30	−4.77	0.17	21 447	2026	4.657	0.074	–	–	1

Table A.4. Observed BCD and apparent parameters of Bn stars.

HD	D_* [dex]	λ_1 [Å]	SpTLC	d [dex]	$E(B-V)$ [mag]	M_V [mag]	σ_{M_V} [mag]	$T_{\rm eff}$ [K]	$\sigma_{T_{\rm eff}}$ [K]	$\log L/L_\odot$ [dex]	$\sigma_{\log L/L_\odot}$ [dex]	$V\sin i$ [km s^{-1}]	$\sigma_{V\sin i}$ [km s^{-1}]	Ref.
HD 560	0.44	63	B9V	0.00	0.03	0.62	0.22	10 666	291	1.862	0.057	249	29	3
HD 5617	0.50	76	A2V	0.00	0.04	0.97	0.51	9151	369	1.619	0.130	236	28	1
HD 10161	0.43	47	B9IV	0.00	0.00	−0.23	0.06	11 187	244	2.237	0.019	160	19	3
HD 10894	0.50	54	A0IV	0.00	0.01	0.21	0.38	9861	285	1.970	0.096	212	30	1
HD 15130	0.52	51	A0-1IV	0.00	0.01	0.36	0.29	9579	209	1.889	0.074	219	26	3
HD 18331	0.49	65	A1V	0.00	0.04	1.05	0.37	9666	367	1.620	0.095	236	28	3
HD 18546	0.49	65	A0-1V	0.00	0.00	0.93	0.29	9666	336	1.667	0.075	–	–	1
HD 21364	0.35	59	B7-8V	0.00	0.04	−0.11	0.26	12 430	475	2.274	0.069	224	26	3
HD 24817	0.50	72	A1-2V	0.00	0.01	1.20	0.52	9242	298	1.534	0.132	285	34	3
HD 26676	0.32	53	B6-7V	0.00	0.12	−0.27	0.35	13 646	536	2.420	0.092	200	24	3

References. $V\sin i$ values taken from: (1) Zorec et al. (2005); (2) Levenhagen & Leister (2006); (3) Zorec & Royer (2012); (4) Frémat et al. (2005); (5) Chauville et al. (2001); (6) Wolff et al. (1982); (7) Abt et al. (2002); (8) Yudin (2001); (9) Slettebak (1982); (10) Uesugi & Fukuda (1982); (11) this work.

Table A.4. continued.

HD	D_* [dex]	λ_1 [Å]	SpTLC	d [dex]	$E(B-V)$ [mag]	M_V [mag]	σ_{M_V} [mag]	$T_{\rm eff}$ [K]	$\sigma_{T_{\rm eff}}$ [K]	$\log L/L_\odot$ [dex]	$\sigma_{\log L/L_\odot}$ [dex]	$V\sin i$ [km s^{-1}]	$\sigma_{V\sin i}$ [km s^{-1}]	Ref.
HD 26793	0.37	50	B7-8IV	abs/0.02	0.02	−0.42	0.35	12 265	390	2.388	0.092	318	38	3
HD 31093	0.48	79	A2IV	0.00	0.01	1.26	0.31	9423	304	1.517	0.079	197	23	11
HD 32039	0.40	58	B9V	0.00	0.02	0.37	0.13	11 551	290	2.025	0.035	343	41	3
HD 32040	0.36	56	B7-8V	0.00	0.03	−0.06	0.14	12 318	332	2.274	0.100	343	41	3
HD 32309	0.46	61	B9.5V	0.00	0.01	0.72	0.24	10 328	346	1.796	0.063	302	36	3
HD 34748	0.15	57	B2V	0.00	0.09	−2.31	0.19	23 529	1546	3.764	0.064	295	35	12
HD 34863	0.32	56	B6-7V	0.00	0.01	−0.20	0.30	13 537	526	2.385	0.080	379	45	3
HD 35407	0.22	58	B4V	0.00	0.03	−1.24	0.10	18 151	595	3.082	0.033	295	35	12
HD 35640	0.43	56	B9IV-V	0.00	0.01	0.10	0.34	11 074	301	2.100	0.088	240	28	3
HD 35656	0.48	77	A1-2VI	0.00	0.00	1.31	0.33	9478	332	1.504	0.085	170	20	13
HD 36058	0.49	56	A0IV	0.00	0.01	0.42	0.28	9973	266	1.894	0.073	210	25	13
HD 45380	0.46	66	A0V	0.00	0.00	0.79	0.22	10 197	342	1.762	0.058	238	28	3
HD 145122	0.50	68	A1V	0.00/0.00	0.01	1.09	0.33	9367	274	1.584	0.084	259	31	3
HD 149485	0.32	55	B6-7V	0.00	0.03	−0.32	0.16	13 576	541	2.436	0.046	354	42	3
HD 158094	0.39	51	B8IV	0.00	0.01	−0.33	0.27	11 884	281	2.327	0.070	265	31	3
HD 159358	0.41	53	B9IV	abs/0.00	0.07	−0.04	0.15	11 491	285	2.185	0.040	240	28	3
HD 160181	0.52	73	A2V	0.00/0.00	0.06	1.10	0.37	8970	260	1.553	0.095	165	19	3
HD 164577	0.53	60	A1IV	0.00	0.03	0.52	0.26	9103	264	1.795	0.066	201	24	3
HD 164900	0.24	50	B4IV	0.00	0.09	−1.49	0.50	16 954	676	3.113	0.130	260	31	7
HD 168905	0.18	57	B2.5V	0.00	0.02	−1.94	0.14	20 901	765	3.499	0.043	248	29	14
HD 171149	0.49	67	A1V	0.00	0.05	0.95	0.34	9593	297	1.656	0.088	301	36	3
HD 172777	0.54	70	A2V	0.00	0.01	1.16	0.39	8970	384	1.529	0.100	149	17	11
HD 177724	0.58	72	A0V	0.00	0.01	0.99	0.23	9810	300	2.044	0.100	317	38	3
HD 177756	0.41	52	B9IV	0.00	0.01	0.06	0.30	11 508	262	2.147	0.077	191	22	3
HD 179648	0.53	59	A1IV	0.02/0.00	0.05	0.51	0.28	9154	293	1.804	0.071	207	24	3
HD 180183	0.17	59	B2.5V	0.00/0.00	0.06	−2.02	0.08	21 746	993	3.572	0.035	215	15	1
HD 180782	0.52	73	A2V	0.00	0.01	1.21	0.38	9230	224	1.526	0.096	212	25	3
HD 181296	0.51	76	A2V	0.00	0.01	1.13	0.54	8974	344	1.542	0.138	420	50	10
HD 182180	0.18	64	B3V	0.00/0.00	0.06	−1.58	0.19	20 927	912	3.358	0.056	320	38	12
HD 182645	0.32	12	A0Ib	0.03/0.00	0.00	−2.93	1.13	10 562	835	2.152	0.100	228	27	3
HD 183537	0.28	47	B5-6IV	0.00/0.00	0.05	−1.37	0.30	15 200	616	2.961	0.080	305	36	7
HD 184606	0.39	57	B8-9V	0.00	0.02	0.21	0.04	11 758	298	2.102	0.016	185	22	12
HD 188293	0.28	57	B5-6V	0.00	0.05	−0.53	0.24	14 895	668	2.608	0.067	271	32	3
HD 190454	0.50	66	A1V	0.00	0.04	0.99	0.33	9444	316	1.628	0.085	310	37	13
HD 195922	0.52	68	A1-2V	0.00	0.05	1.04	0.41	9100	467	1.586	0.105	201	24	3
HD 198529	0.50	61	A0-1IV-V	0.00	0.02	0.60	0.43	9594	301	1.795	0.110	275	33	11
HD 199280	0.38	51	B8IV	0.00	0.02	−0.44	0.28	12 064	327	2.384	0.071	265	31	3
HD 208321	0.53	60	A1IV	0.00	0.04	0.43	0.23	9103	415	1.830	0.062	216	25	11
HD 210419	0.48	60	A0IV-V	0.00/0.00	0.01	0.59	0.32	9965	310	1.822	0.083	322	38	3
HD 213998	0.43	57	B9IV-V	0.00	0.02	0.31	0.15	11 042	301	2.012	0.041	271	32	3
HD 215143	0.48	62	A0IV-V	0.00	0.00	0.83	0.36	9921	353	1.725	0.094	205	24	3
HD 218639	0.50	70	A1V	0.00	0.01	1.04	0.31	9288	339	1.597	0.079	269	32	3
HD 219659	0.49	66	A0-1V	0.00	0.04	0.88	0.27	9630	303	1.684	0.071	196	23	3
HD 222847	0.39	55	B8-9IV-V	0.00	0.01	−0.01	0.14	11 811	281	2.192	0.037	302	36	3
HD 223785	0.51	77	A2V	0.00	0.01	1.26	0.48	8948	319	1.489	0.123	199	16	1

Table A.5. Derived apparent fundamental parameters of Be stars.

HD	$M/M_\odot$	$\sigma_{M/M_\odot}$	$\log g$ [dex]	$\sigma_{\log g}$ [dex]	$R/R_\odot$	$\sigma_{R/R_\odot}$	$V_{\rm c}$ [km s^{-1}]	$\sigma_{V_{\rm c}}$ [km s^{-1}]	$t/t_{\rm MS}$	$\sigma_{t/t_{\rm MS}}$
HD 10144	6.94	0.18	3.55	0.09	7.32	1.96	350	51	1.019	0.006
HD 16582	10.37	0.61	3.79	0.13	6.79	2.24	445	86	0.886	0.114
HD 23016	3.66	0.07	3.87	0.04	3.68	0.31	359	18	0.880	0.054
HD 28248	7.14	0.35	4.06	0.14	4.13	1.65	476	71	0.581	0.240
HD 28497	16.06	0.89	4.05	0.11	6.22	1.55	584	89	0.510	0.193
HD 30076	16.84	1.04	3.09	0.13	19.29	7.98	335	79	1.019	0.001
HD 30739	2.37	0.09	3.84	0.10	3.06	0.50	316	31	0.933	0.092
HD 31209	2.55	0.08	3.83	0.07	3.21	0.36	320	22	0.940	0.078
HD 35165	5.49	0.10	4.05	0.05	3.67	0.50	442	33	0.668	0.076
HD 35411	14.69	0.91	4.01	0.13	6.24	1.84	557	99	0.583	0.202
HD 35468	11.81	0.46	3.33	0.11	12.22	4.33	353	69	1.025	0.001
HD 36012	5.20	0.10	4.06	0.05	3.53	0.44	439	31	0.655	0.078

Table A.5. continued.

HD	$M/M_\odot$	$\sigma_{M/M_\odot}$	$\log g$ [dex]	$\sigma_{\log g}$ [dex]	$R/R_\odot$	$\sigma_{R/R_\odot}$	V_c [km s^{-1}]	σ_{V_c} [km s^{-1}]	t/t_{MS}	$\sigma_{t/t_{MS}}$
HD 36861	20.21	2.49	3.35	0.14	15.56	4.69	409	86	1.006	0.018
HD 37490	12.06	0.72	3.28	0.12	13.09	4.81	344	73	1.025	0.001
HD 37971	5.74	0.09	3.87	0.05	4.58	0.60	403	29	0.860	0.046
HD 42327	2.71	0.05	4.06	0.05	2.56	0.28	371	23	0.682	0.064
HD 43445	3.44	0.07	3.90	0.05	3.44	0.32	360	20	0.847	0.049
HD 44783	3.81	0.13	3.86	0.09	3.79	0.59	361	34	0.888	0.092
HD 44996	6.37	0.14	4.07	0.06	3.83	0.68	467	46	0.603	0.108
HD 45871	5.56	0.19	4.13	0.09	3.35	0.65	467	53	0.508	0.167
HD 47054	3.59	0.08	3.94	0.05	3.29	0.45	376	29	0.785	0.061
HD 49131	10.78	0.47	3.88	0.11	6.19	1.79	476	79	0.798	0.120
HD 52089	12.27	0.71	4.09	0.13	5.24	1.75	557	84	0.483	0.246
HD 56139	8.59	0.27	3.70	0.08	6.82	1.30	403	44	0.973	0.053
HD 57150	11.22	0.47	3.45	0.12	10.38	3.82	373	76	1.020	0.008
HD 58155	6.07	0.22	4.06	0.10	3.78	0.85	458	60	0.613	0.158
HD 58343	6.43	0.18	4.14	0.07	3.56	0.56	488	45	0.472	0.146
HD 60606	11.10	0.41	3.52	0.12	9.55	3.43	387	76	1.014	0.019
HD 61224	5.31	0.18	3.68	0.09	5.49	1.36	353	49	1.003	0.047
HD 65875	11.28	0.55	4.10	0.11	4.96	0.94	548	65	0.485	0.209
HD 66194	8.98	0.49	3.93	0.13	5.35	1.58	468	81	0.754	0.159
HD 71072	6.35	0.21	3.81	0.09	5.16	1.22	399	53	0.912	0.086
HD 78764	12.26	0.79	3.69	0.14	8.22	2.77	439	88	0.936	0.093
HD 86440	7.99	0.34	3.44	0.12	8.90	3.33	340	70	1.019	0.003
HD 88825	6.68	0.16	3.59	0.09	6.89	1.87	354	52	1.018	0.008
HD 89080	4.73	0.14	3.63	0.09	5.48	1.33	333	45	1.025	0.019
HD 89884	4.13	0.12	4.00	0.09	3.35	0.78	401	52	0.726	0.112
HD 90490	4.61	0.11	4.08	0.07	3.25	0.58	430	43	0.626	0.111
HD 91120	2.52	0.06	4.05	0.06	2.48	0.32	363	27	0.694	0.075
HD 91465	9.88	0.34	3.92	0.08	5.73	1.07	474	52	0.778	0.086
HD 102776	8.01	0.25	4.11	0.08	4.12	0.77	506	55	0.508	0.153
HD 124367	6.37	0.20	4.06	0.08	3.91	0.62	462	43	0.628	0.121
HD 127449	6.65	0.22	4.10	0.08	3.80	0.74	480	54	0.544	0.157
HD 131492	11.40	0.63	3.78	0.13	7.14	2.27	455	84	0.884	0.110
HD 135734	3.49	0.14	3.99	0.09	3.14	0.56	380	41	0.749	0.110
HD 137387	11.44	0.46	3.97	0.11	5.77	1.67	510	84	0.686	0.143
HD 138769	6.12	0.16	4.17	0.07	3.37	0.60	490	50	0.424	0.154
HD 142184	8.04	0.23	4.11	0.07	4.16	0.80	504	55	0.522	0.142
HD 142983	4.79	0.11	4.03	0.07	3.50	0.60	423	41	0.697	0.093
HD 148259	18.93	1.04	3.93	0.13	7.81	2.82	564	85	0.659	0.165
HD 154243	10.50	0.37	4.00	0.09	5.39	1.37	505	73	0.670	0.131
HD 155436	23.27	2.43	3.21	0.17	19.58	9.72	391	59	1.006	0.017
HD 165910	2.75	0.06	3.87	0.06	3.18	0.34	335	21	0.888	0.068
HD 166182	6.88	0.19	3.88	0.08	4.96	1.01	424	48	0.840	0.083
HD 166566	27.38	3.29	3.44	0.19	16.31	8.89	466	70	0.916	0.088
HD 171054	11.21	0.41	3.48	0.12	10.05	3.62	379	75	1.019	0.009
HD 171623	2.72	0.06	3.90	0.06	3.07	0.37	339	23	0.863	0.066
HD 176304	7.69	0.25	3.65	0.10	6.84	1.92	381	59	0.994	0.043
HD 178744	4.79	0.15	3.91	0.07	4.04	0.42	392	26	0.841	0.068
HD 187567	9.54	0.27	4.08	0.06	4.64	0.61	520	41	0.550	0.120
HD 187811	7.20	0.22	4.04	0.08	4.25	0.86	471	55	0.645	0.124
HD 192044	4.75	0.15	3.79	0.08	4.60	0.95	365	43	0.953	0.073
HD 193911	3.90	0.13	3.88	0.08	3.76	0.56	366	33	0.872	0.088
HD 205637	13.26	0.69	2.97	0.14	19.60	8.40	295	71	1.024	0.001
HD 208057	4.84	0.17	4.07	0.09	3.38	0.61	433	46	0.637	0.138
HD 209014	3.46	0.06	3.96	0.06	3.24	0.50	372	32	0.790	0.060
HD 209409	4.72	0.14	3.80	0.08	4.52	0.85	367	40	0.943	0.074
HD 209522	6.38	0.18	3.80	0.07	5.25	0.84	397	37	0.923	0.070
HD 210129	4.59	0.13	3.93	0.06	3.87	0.53	393	32	0.820	0.067
HD 212076	18.71	2.08	3.38	0.20	14.40	8.04	410	62	0.989	0.052
HD 217891	4.83	0.13	3.90	0.07	4.09	0.60	391	34	0.849	0.069
HD 225132	2.99	0.06	3.86	0.04	3.35	0.35	340	21	0.892	0.062
HD 256577	14.61	0.55	3.22	0.12	15.43	5.83	349	72	1.021	0.001

Table A.6. Derived apparent fundamental parameters of Bn stars.

HD	$M/M_\odot$	$\sigma_{M/M_\odot}$	$\log g$ [dex]	$\sigma_{\log g}$ [dex]	$R/R_\odot$	$\sigma_{R/R_\odot}$	V_c [km s^{-1}]	σ_{V_c} [km s^{-1}]	t/t_{MS}	$\sigma_{t/t_{MS}}$
HD 560	2.74	0.05	4.08	0.05	2.50	0.27	378	24	0.647	0.068
HD 5617	2.34	0.09	3.99	0.09	2.57	0.42	344	34	0.777	0.105
HD 10161	3.30	0.04	3.87	0.03	3.50	0.31	349	17	0.881	0.042
HD 10894	2.79	0.07	3.84	0.07	3.31	0.39	330	23	0.920	0.077
HD 15130	2.67	0.06	3.86	0.05	3.20	0.28	329	18	0.912	0.068
HD 18331	2.38	0.07	4.09	0.07	2.30	0.35	367	33	0.642	0.105
HD 18546	2.43	0.06	4.05	0.06	2.43	0.34	361	29	0.696	0.078
HD 21364	3.47	0.08	4.04	0.06	2.96	0.45	391	34	0.691	0.084
HD 24817	2.26	0.09	4.08	0.08	2.28	0.30	359	31	0.666	0.117
HD 26676	3.85	0.11	4.10	0.07	2.90	0.46	416	38	0.593	0.121
HD 26793	3.63	0.10	3.92	0.07	3.46	0.44	369	28	0.829	0.072
HD 31093	2.26	0.05	4.13	0.06	2.15	0.28	370	28	0.595	0.099
HD 32039	3.03	0.04	4.10	0.04	2.57	0.26	392	22	0.608	0.061
HD 32040	3.46	0.11	4.02	0.06	3.01	0.33	387	27	0.713	0.083
HD 32309	2.63	0.05	4.07	0.05	2.47	0.33	372	28	0.660	0.077
HD 34748	9.33	0.39	4.08	0.10	4.59	1.21	517	78	0.535	0.190
HD 34863	3.78	0.09	4.11	0.07	2.83	0.44	418	37	0.573	0.117
HD 35407	5.90	0.10	4.12	0.05	3.51	0.46	469	34	0.542	0.093
HD 35640	3.09	0.09	3.96	0.06	3.05	0.33	363	25	0.787	0.061
HD 35656	2.25	0.06	4.15	0.07	2.10	0.30	374	31	0.557	0.115
HD 36058	2.72	0.07	3.93	0.05	2.96	0.32	345	23	0.827	0.053
HD 45380	2.58	0.05	4.08	0.05	2.44	0.33	371	28	0.658	0.075
HD 145122	2.32	0.06	4.06	0.06	2.35	0.28	358	26	0.691	0.078
HD 149485	3.86	0.07	4.07	0.06	2.99	0.48	411	36	0.634	0.090
HD 158094	3.50	0.08	3.91	0.05	3.44	0.33	363	21	0.838	0.049
HD 159358	3.25	0.04	3.96	0.04	3.12	0.31	368	20	0.787	0.040
HD 160181	2.26	0.07	4.01	0.06	2.47	0.29	344	25	0.764	0.070
HD 164577	2.51	0.06	3.83	0.06	3.18	0.37	319	22	0.944	0.070
HD 164900	5.75	0.24	3.96	0.09	4.17	0.67	423	42	0.772	0.102
HD 168905	7.66	0.16	4.06	0.06	4.28	0.63	484	40	0.616	0.092
HD 171149	2.41	0.07	4.05	0.06	2.44	0.31	359	27	0.703	0.079
HD 172777	2.24	0.07	4.02	0.08	2.41	0.42	347	35	0.742	0.098
HD 177724	2.85	0.08	3.77	0.07	3.64	0.45	318	24	0.980	0.058
HD 177756	3.19	0.08	3.99	0.05	2.98	0.27	373	21	0.749	0.058
HD 179648	2.52	0.07	3.84	0.06	3.17	0.41	320	25	0.938	0.073
HD 180183	8.12	0.21	4.08	0.07	4.30	0.79	498	51	0.572	0.120
HD 180782	2.25	0.07	4.08	0.06	2.27	0.23	359	23	0.667	0.086
HD 181296	2.25	0.10	4.01	0.09	2.44	0.38	346	34	0.750	0.112
HD 182180	7.28	0.21	4.18	0.07	3.63	0.63	515	52	0.379	0.160
HD 182645	3.08	0.12	3.82	0.12	3.56	1.13	335	59	0.917	0.104
HD 183537	5.09	0.14	3.87	0.07	4.36	0.71	389	36	0.880	0.072
HD 184606	3.15	0.03	4.07	0.03	2.71	0.28	389	21	0.651	0.050
HD 188293	4.34	0.11	4.11	0.07	3.02	0.54	433	44	0.563	0.126
HD 190454	2.37	0.06	4.04	0.06	2.43	0.33	356	28	0.714	0.079
HD 195922	2.30	0.08	4.00	0.09	2.50	0.52	346	42	0.760	0.107
HD 198529	2.57	0.09	3.94	0.07	2.86	0.36	341	27	0.827	0.080
HD 199280	3.60	0.08	3.89	0.05	3.56	0.39	362	23	0.862	0.065
HD 208321	2.54	0.07	3.80	0.07	3.31	0.61	315	33	0.960	0.070
HD 210419	2.63	0.07	3.98	0.06	2.73	0.34	353	26	0.770	0.064
HD 213998	2.96	0.04	4.02	0.04	2.77	0.30	373	22	0.716	0.051
HD 215143	2.51	0.07	4.05	0.07	2.47	0.36	364	31	0.687	0.090
HD 218639	2.33	0.06	4.03	0.06	2.43	0.36	353	30	0.725	0.078
HD 219659	2.45	0.06	4.03	0.05	2.50	0.32	357	27	0.723	0.068
HD 222847	3.28	0.04	4.01	0.04	2.98	0.28	378	20	0.736	0.043
HD 223785	2.20	0.08	4.05	0.08	2.31	0.34	352	32	0.705	0.106

Table A.7. Hα line emission equivalent widths and fluxes of Be stars.

HD	W_e [Å]	W [Å]	$F_{H\alpha}/10^9$ [cgs]	d [dex]
HD 10144	−2.83	1.50	0.033	0.03
HD 23016	−4.53	4.44	0.068	0.00
HD 28497	7.42	10.07	0.692	−0.06
HD 28497	14.25	16.90	1.161	−0.03
HD 30076	6.62	9.01	0.299	0.00
HD 30076	37.21	39.60	1.312	−0.07
HD 30739	−8.22	5.04	0.035	0.00
HD 31209	−3.11	−0.65	−0.005	0.03
HD 35165	4.79	10.39	0.231	0.10
HD 35411	−3.25	−0.26	−0.014	−0.03
HD 35411	−3.40	−0.41	−0.022	0.00
HD 36012	27.32	33.32	0.741	−0.03
HD 37490	10.96	13.56	0.355	−0.03
HD 37971	−5.20	0.80	0.018	0.00
HD 42327	−4.95	−0.44	−0.005	0.00
HD 43445	−0.43	2.34	0.028	0.04
HD 44783	3.69	12.66	0.194	0.05
HD 44996	3.94	8.86	0.232	−0.02
HD 44996	−0.43	4.50	0.118	0.00
HD 45871	0.99	6.23	0.139	0.00
HD 47054	3.39	12.36	0.190	0.00
HD 47054	5.91	14.88	0.228	0.00
HD 49131	−2.23	1.56	0.060	0.00
HD 56139	5.72	9.29	0.308	0.00
HD 56139	21.52	25.09	0.831	−0.06
HD 57150	33.99	37.36	1.237	−0.05
HD 58155	−1.22	−0.01	0.001	0.00
HD 58343	3.19	8.12	0.212	−0.06
HD 60606	6.93	10.10	0.335	−0.02
HD 61224	3.31	8.34	0.156	0.00
HD 65875	11.51	14.92	0.813	−0.06
HD 66194	3.82	8.03	0.266	−0.04
HD 71072	−0.77	−0.07	−0.002	0.02
HD 78764	1.04	3.81	0.146	0.00
HD 88825	6.41	10.74	0.239	0.00
HD 89080	2.79	8.87	0.136	0.05
HD 89884	7.40	14.48	0.222	0.00
HD 90490	4.99	11.47	0.214	0.00
HD 91120	1.42	14.68	0.126	0.00
HD 91465	7.57	11.57	0.443	−0.03
HD 102776	3.93	8.35	0.276	0.00
HD 124367	22.21	27.14	0.710	−0.04
HD 127449	8.89	13.82	0.362	0.00
HD 131492	0.03	3.82	0.146	−0.04
HD 135734	3.40	12.37	0.190	0.00
HD 137387	−1.84	1.75	0.095	0.00
HD 138769	−5.33	−0.40	−0.011	0.00
HD 142184	−3.51	0.70	0.023	0.00
HD 142983	24.79	31.28	0.584	0.14
HD 148259	39.69	42.14	2.895	−0.05
HD 155436	6.81	8.28	0.452	0.00
HD 165910	−5.58	−0.07	−0.001	0.00
HD 166566	4.94	6.75	0.368	0.00
HD 171623	−5.33	−0.46	−0.004	0.00
HD 176304	−3.14	0.89	0.023	0.00
HD 187567	21.96	25.75	0.986	−0.05
HD 187811	−3.61	1.04	0.034	−0.02
HD 192044	9.54	16.62	0.311	0.03
HD 193911	6.05	13.91	0.213	0.04
HD 205637	1.56	4.57	0.102	0.08
HD 208057	−5.42	0.58	0.011	0.00
HD 209014	5.72	7.65	0.117	0.00
HD 209014	5.37	14.34	0.220	0.02
HD 209409	16.45	23.53	0.440	0.00
HD 209409	20.63	27.71	0.518	0.02
HD 209522	−4.98	0.62	0.014	0.00
HD 210129	−0.96	6.12	0.114	−0.02
HD 212076	9.67	12.14	0.662	−0.03
HD 217891	14.25	20.73	0.387	0.00
HD 225132	−4.48	2.45	0.025	0.02
HD 256577	−3.07	−0.68	−0.022	0.00

Table A.7. continued.

Table A.8. Parent nonrotating counterpart (pnrc) fundamental parameters of Be stars.

HD	$T_{\rm eff}$ [K]	$\sigma_{T_{\rm eff}}$ [K]	$\log L/L_\odot$ [dex]	$\sigma_{\log L/L_\odot}$ [dex]	$\log g$ [dex]	$\sigma_{\log g}$ [dex]	$M/M_\odot$	$\sigma_{M/M_\odot}$	$V\sin i$ [km s^{-1}]	$\sigma_{V\sin i}$ [km s^{-1}]	$V_{\rm c}$ [km s^{-1}]	$\sigma_{V_{\rm c}}$ [km s^{-1}]	$t/t_{\rm MS}$	$\sigma_{t/t_{\rm MS}}$
HD 10144	18 698	1458	3.614	0.080	3.74	0.12	7.48	0.32	269	32	398	29	0.946	0.080
HD 16582	23 587	2481	3.869	0.129	4.00	0.16	9.78	0.65	13	1	501	55	0.632	0.256
HD 23016	14 066	472	2.551	0.077	4.05	0.06	4.12	0.10	320	38	411	14	0.671	0.088
HD 28248	20 659	2636	3.207	0.055	4.25	0.16	6.43	0.66	33	4	521	56	0.263	0.284
HD 28497	32 749	2486	4.406	0.112	4.24	0.11	15.75	0.98	352	42	654	40	0.162	0.192
HD 30076	23 915	3026	4.908	0.155	3.25	0.17	18.16	1.54	270	32	376	36	1.014	0.008
HD 30739	9794	493	1.801	0.264	3.97	0.16	2.59	0.19	238	28	349	27	0.771	0.191
HD 31209	10 684	406	1.964	0.122	4.00	0.08	2.87	0.11	286	34	365	15	0.739	0.096
HD 35165	19 680	911	3.131	0.077	4.23	0.07	6.27	0.43	401	48	513	23	0.258	0.176
HD 35411	30 247	2794	4.239	0.133	4.21	0.13	13.59	1.22	182	21	616	49	0.247	0.252
HD 35468	20 928	2356	4.173	0.082	3.52	0.15	10.52	0.43	47	5	383	33	1.008	0.032
HD 36012	17 481	683	2.810	0.056	4.27	0.06	5.18	0.13	210	25	499	19	0.228	0.149
HD 36861	26 853	2544	4.818	0.221	3.53	0.17	17.77	1.90	78	9	440	40	0.961	0.073
HD 37490	21 196	2370	4.288	0.129	3.46	0.15	11.38	0.67	173	20	377	33	1.015	0.025
HD 37971	16 977	707	2.958	0.042	4.08	0.06	5.38	0.11	24	2	450	18	0.608	0.103
HD 42327	12 716	517	2.096	0.082	4.23	0.07	3.27	0.09	383	45	432	18	0.355	0.152
HD 43445	13 306	456	2.380	0.076	4.08	0.06	3.74	0.09	295	35	409	14	0.623	0.097
HD 44783	13 952	685	2.531	0.131	4.05	0.10	4.08	0.16	273	32	411	22	0.658	0.143
HD 44996	19 415	1099	3.036	0.031	4.27	0.05	5.76	0.48	42	5	512	19	0.166	0.162
HD 45871	19 180	1127	2.954	0.102	4.30	0.07	5.46	0.44	312	37	517	19	0.120	0.153
HD 47054	13 515	583	2.345	0.060	4.13	0.06	3.81	0.11	266	32	422	16	0.494	0.104
HD 49131	25 697	2273	3.976	0.085	4.09	0.13	10.86	0.73	262	31	542	47	0.482	0.256
HD 52089	28 081	2979	3.946	0.089	4.27	0.13	10.83	1.18	38	4	603	51	0.173	0.225
HD 56139	20 901	1258	3.671	0.085	3.92	0.09	8.23	0.29	101	12	453	27	0.790	0.108
HD 57150	23 331	2576	4.298	0.109	3.64	0.16	11.88	0.73	281	33	423	42	0.960	0.084
HD 58155	19 640	1345	3.092	0.108	4.24	0.09	5.95	0.60	281	33	509	25	0.225	0.213
HD 58343	19 913	995	3.016	0.078	4.31	0.05	5.53	0.56	54	6	521	16	0.067	0.102
HD 60606	24 268	2562	4.308	0.103	3.71	0.15	12.21	0.77	312	37	444	44	0.921	0.108
HD 61224	16 268	1236	3.106	0.085	3.88	0.11	5.60	0.22	244	29	402	28	0.855	0.116
HD 65875	27 232	1630	3.857	0.150	4.28	0.09	10.17	1.13	174	20	597	26	0.117	0.166
HD 66194	23 676	2139	3.711	0.148	4.14	0.15	9.13	0.67	268	32	533	50	0.420	0.280
HD 71072	19 390	1354	3.374	0.086	4.01	0.11	6.94	0.26	311	37	459	31	0.679	0.152
HD 78764	25 296	2668	4.172	0.143	3.90	0.17	11.79	0.83	160	19	494	53	0.749	0.204
HD 86440	17 699	2108	3.607	0.098	3.63	0.16	7.29	0.37	24	2	374	38	0.977	0.070
HD 88825	17 379	1476	3.371	0.054	3.79	0.12	6.47	0.26	140	16	396	31	0.919	0.098
HD 89080	15 531	1186	3.062	0.094	3.82	0.12	5.36	0.22	289	34	385	28	0.908	0.103
HD 89884	15 337	1090	2.581	0.092	4.19	0.11	4.36	0.18	289	34	456	30	0.395	0.224
HD 90490	16 026	899	2.575	0.067	4.28	0.07	4.39	0.22	145	17	481	20	0.207	0.176
HD 91120	10 873	443	1.722	0.082	4.23	0.07	2.61	0.07	245	29	409	17	0.372	0.152
HD 91465	25 092	1441	3.880	0.093	4.12	0.10	10.32	0.44	304	36	545	35	0.449	0.204
HD 102776	23 323	1347	3.455	0.073	4.29	0.06	7.58	0.58	287	34	556	17	0.102	0.135
HD 124367	20 588	998	3.220	0.105	4.24	0.07	6.53	0.73	329	39	519	25	0.218	0.183
HD 127449	21 836	1295	3.312	0.089	4.29	0.09	7.20	0.27	–	–	551	27	0.140	0.163
HD 131492	25 346	2487	4.062	0.109	3.99	0.15	11.25	0.69	202	24	516	52	0.636	0.231
HD 135734	13 943	790	2.386	0.138	4.17	0.10	3.83	0.20	317	38	434	26	0.453	0.210
HD 137387	27 048	2414	3.998	0.066	4.17	0.12	11.33	0.85	265	31	577	49	0.321	0.263
HD 138769	19 516	1108	2.937	0.054	4.34	0.05	5.31	0.39	103	12	524	13	0.050	0.084
HD 142184	23 683	1396	3.504	0.056	4.27	0.05	7.76	0.69	331	39	555	17	0.111	0.140
HD 142983	18 734	1039	3.035	0.090	4.21	0.08	5.86	0.33	443	53	498	25	0.314	0.203
HD 148259	32 542	3709	4.552	0.065	4.11	0.15	16.91	1.50	95	11	616	61	0.359	0.292
HD 154243	26 153	2047	3.884	0.053	4.19	0.09	10.25	0.77	278	33	566	34	0.283	0.240
HD 155436	27 853	3915	5.160	0.188	3.38	0.20	23.89	3.05	274	32	435	54	0.958	0.072
HD 165910	11 205	400	2.054	0.167	4.02	0.10	3.04	0.15	276	33	374	19	0.710	0.132
HD 166182	19 159	1239	3.237	0.071	4.10	0.10	6.52	0.23	35	4	477	31	0.546	0.181
HD 166566	30 303	5180	5.069	0.160	3.60	0.24	23.16	2.73	71	8	494	78	0.858	0.151
HD 171054	21 944	2509	4.085	0.078	3.68	0.16	10.26	0.57	46	5	418	43	0.946	0.092
HD 171623	11 515	467	2.059	0.087	4.07	0.07	3.07	0.08	309	37	386	15	0.652	0.103

Table A.8. continued.

HD	$T_{\rm eff}$ [K]	$\sigma_{T_{\rm eff}}$ [K]	$\log L/L_\odot$ [dex]	$\sigma_{\log L/L_\odot}$ [dex]	$\log g$ [dex]	$\sigma_{\log g}$ [dex]	$M/M_\odot$	$\sigma_{M/M_\odot}$	$V\sin i$ [km s^{-1}]	$\sigma_{V\sin i}$ [km s^{-1}]	$V_{\rm c}$ [km s^{-1}]	$\sigma_{V_{\rm c}}$ [km s^{-1}]	$t/t_{\rm MS}$	$\sigma_{t/t_{\rm MS}}$
HD 176304	19 089	1701	3.510	0.064	3.86	0.13	7.25	0.31	48	5	426	35	0.847	0.129
HD 178744	15 994	542	2.793	0.108	4.10	0.08	4.86	0.15	237	28	443	18	0.582	0.132
HD 187567	24 832	1036	3.637	0.078	4.29	0.07	9.05	0.60	150	18	584	25	0.100	0.122
HD 187811	21 485	1334	3.341	0.075	4.24	0.09	7.28	0.30	267	32	536	30	0.238	0.202
HD 192044	15 900	1025	2.929	0.087	3.98	0.10	5.14	0.17	280	33	418	25	0.751	0.121
HD 193911	13 691	636	2.457	0.118	4.07	0.09	3.92	0.14	207	24	413	21	0.625	0.141
HD 205637	20 620	2548	4.686	0.144	3.13	0.16	14.95	1.11	265	31	334	29	1.021	0.001
HD 208057	16 423	938	2.648	0.116	4.26	0.08	4.55	0.33	126	15	481	22	0.236	0.201
HD 209014	13 624	690	2.368	0.070	4.14	0.08	3.77	0.10	304	36	425	20	0.522	0.145
HD 209409	15 928	944	2.917	0.091	3.99	0.09	5.12	0.17	284	34	421	23	0.736	0.116
HD 209522	19 408	958	3.391	0.091	4.00	0.08	6.98	0.23	313	37	456	23	0.705	0.113
HD 210129	15 431	669	2.679	0.087	4.13	0.08	4.56	0.13	201	24	442	20	0.540	0.141
HD 212076	26 507	4631	4.735	0.207	3.56	0.25	16.86	1.96	118	14	446	70	0.919	0.129
HD 217891	15 417	718	2.702	0.084	4.10	0.08	4.60	0.13	97	11	438	21	0.578	0.136
HD 225132	11 453	388	2.068	0.052	4.05	0.05	3.07	0.05	229	27	382	11	0.681	0.071
HD 256577	23 891	2708	4.685	0.074	3.40	0.15	15.22	0.65	–	–	391	34	1.012	0.010

Table A.9. Parent nonrotating counterpart (pnrc) fundamental parameters of Bn stars.

HD	$T_{\rm eff}$ [K]	$\sigma_{T_{\rm eff}}$ [K]	$\log L/L_\odot$ [dex]	$\sigma_{\log L/L_\odot}$ [dex]	$\log g$ [dex]	$\sigma_{\log g}$ [dex]	$M/M_\odot$	$\sigma_{M/M_\odot}$	$V\sin i$ [km s^{-1}]	$\sigma_{V\sin i}$ [km s^{-1}]	$V_{\rm c}$ [km s^{-1}]	$\sigma_{V_{\rm c}}$ [km s^{-1}]	$t/t_{\rm MS}$	$\sigma_{t/t_{\rm MS}}$
HD 560	11 719	427	1.921	0.069	4.21	0.06	2.92	0.06	258	31	416	15	0.399	0.128
HD 5617	10 128	524	1.701	0.137	4.11	0.10	2.51	0.10	244	29	377	20	0.590	0.163
HD 10161	11 825	332	2.193	0.026	4.01	0.04	3.29	0.03	170	20	379	8	0.734	0.046
HD 10894	10 809	412	2.023	0.103	3.98	0.07	2.96	0.10	220	26	362	14	0.770	0.085
HD 15130	10 560	327	1.957	0.084	3.98	0.06	2.85	0.08	226	27	361	11	0.763	0.065
HD 18331	10 577	513	1.672	0.102	4.22	0.08	2.51	0.11	245	29	402	19	0.398	0.178
HD 18546	10 586	456	1.719	0.075	4.18	0.07	2.57	0.06	–	–	396	16	0.475	0.136
HD 21364	13 445	661	2.289	0.076	4.18	0.08	3.63	0.10	241	28	431	21	0.449	0.158
HD 24817	10 521	470	1.687	0.143	4.20	0.10	2.52	0.13	292	35	397	20	0.437	0.194
HD 26676	14 491	711	2.387	0.095	4.24	0.08	3.87	0.26	217	26	454	21	0.303	0.184
HD 26793	14 232	596	2.577	0.102	4.05	0.08	4.19	0.13	322	38	414	18	0.663	0.116
HD 31093	10 068	414	1.508	0.083	4.26	0.07	2.31	0.07	207	24	403	16	0.321	0.164
HD 32039	13 394	479	2.214	0.056	4.23	0.06	3.52	0.07	344	41	442	15	0.340	0.128
HD 32040	14 345	515	2.472	0.107	4.15	0.08	4.03	0.12	344	41	436	19	0.490	0.151
HD 32309	11 813	535	1.956	0.082	4.20	0.08	2.98	0.08	308	37	415	18	0.422	0.152
HD 34748	25 189	2029	3.752	0.071	4.22	0.10	9.47	0.49	303	36	566	36	0.245	0.235
HD 34863	15 802	769	2.588	0.088	4.25	0.08	4.44	0.18	379	45	473	22	0.284	0.183
HD 35407	19 802	830	3.118	0.050	4.26	0.06	6.27	0.41	313	37	520	21	0.202	0.148
HD 35640	12 193	448	2.163	0.096	4.09	0.07	3.29	0.10	249	29	399	16	0.610	0.113
HD 35656	9987	444	1.459	0.087	4.28	0.07	2.23	0.11	180	21	405	14	0.267	0.174
HD 36058	10 844	381	1.927	0.080	4.06	0.06	2.83	0.07	218	26	377	13	0.670	0.087
HD 45380	11 156	482	1.811	0.069	4.21	0.07	2.73	0.06	247	29	408	17	0.417	0.141
HD 145122	10 461	419	1.688	0.096	4.18	0.07	2.53	0.07	267	32	394	16	0.470	0.145
HD 149485	15 732	802	2.621	0.064	4.21	0.08	4.51	0.12	361	43	465	23	0.363	0.175
HD 158094	13 348	463	2.438	0.084	4.04	0.06	3.84	0.10	276	33	402	14	0.683	0.090
HD 159358	12 635	431	2.243	0.055	4.09	0.05	3.45	0.06	251	30	404	13	0.609	0.087
HD 160181	9504	351	1.522	0.097	4.14	0.07	2.27	0.07	175	21	373	14	0.570	0.123
HD 164577	9944	378	1.841	0.075	3.97	0.06	2.66	0.07	209	25	351	11	0.789	0.065
HD 164900	18 526	924	3.153	0.136	4.10	0.10	6.17	0.26	282	33	471	28	0.548	0.186
HD 168905	22 189	1015	3.464	0.049	4.21	0.07	7.92	0.27	257	30	537	25	0.292	0.170
HD 171149	11 046	471	1.836	0.101	4.17	0.08	2.75	0.08	305	36	399	18	0.490	0.148
HD 172777	9427	509	1.477	0.102	4.16	0.09	2.22	0.07	160	19	376	19	0.528	0.166
HD 177724	11 554	423	2.271	0.101	3.90	0.07	3.37	0.10	317	34	358	14	0.850	0.082
HD 177756	12 272	367	2.127	0.081	4.13	0.06	3.25	0.08	202	24	407	13	0.544	0.105

Table A.9. continued.

HD	$T_{\rm eff}$ [K]	$\sigma_{T_{\rm eff}}$ [K]	$\log L/L_\odot$ [dex]	$\sigma_{\log L/L_\odot}$ [dex]	$\log g$ [dex]	$\sigma_{\log g}$ [dex]	$M/M_\odot$	$\sigma_{M/M_\odot}$	$V\sin i$ [km s^{-1}]	$\sigma_{V\sin i}$ [km s^{-1}]	$V_{\rm c}$ [km s^{-1}]	$\sigma_{V_{\rm c}}$ [km s^{-1}]	$t/t_{\rm MS}$	$\sigma_{t/t_{\rm MS}}$
HD 179648	10 038	417	1.860	0.080	3.97	0.07	2.68	0.07	214	25	352	13	0.787	0.076
HD 180183	22 795	1306	3.503	0.038	4.22	0.07	8.04	0.47	222	26	544	27	0.241	0.191
HD 180782	9979	323	1.551	0.101	4.21	0.07	2.34	0.07	222	26	392	15	0.434	0.147
HD 181296	10 594	487	1.780	0.138	4.13	0.10	2.64	0.11	420	38	420	20	0.550	0.165
HD 182180	22 686	1224	3.378	0.066	4.30	0.06	7.37	0.39	331	39	558	17	0.091	0.122
HD 182645	11 696	1132	2.230	0.110	3.95	0.14	3.32	0.14	236	28	369	31	0.779	0.169
HD 183537	17 436	914	3.122	0.095	4.00	0.09	5.86	0.20	327	39	438	23	0.710	0.116
HD 184606	12 454	407	2.064	0.026	4.21	0.05	3.19	0.04	197	23	426	12	0.393	0.097
HD 188293	16 298	921	2.652	0.077	4.25	0.08	4.60	0.25	291	34	478	23	0.266	0.192
HD 190454	10 941	481	1.821	0.096	4.16	0.08	2.72	0.08	310	37	397	18	0.503	0.144
HD 195922	9827	630	1.605	0.110	4.13	0.10	2.38	0.08	210	25	377	22	0.561	0.177
HD 198529	10 974	478	1.956	0.122	4.06	0.09	2.89	0.11	280	33	378	17	0.663	0.121
HD 199280	13 572	517	2.498	0.085	4.02	0.07	3.96	0.11	277	33	401	15	0.705	0.091
HD 208321	10 081	579	1.911	0.075	3.93	0.08	2.74	0.07	223	26	347	17	0.823	0.097
HD 210419	11 631	464	2.030	0.091	4.11	0.07	3.04	0.09	322	37	395	16	0.585	0.117
HD 213998	12 348	464	2.114	0.061	4.16	0.06	3.24	0.07	279	33	413	15	0.504	0.112
HD 215143	10 672	482	1.731	0.098	4.19	0.08	2.59	0.08	215	25	398	18	0.460	0.158
HD 218639	10 488	506	1.729	0.094	4.16	0.08	2.57	0.08	276	33	390	18	0.520	0.148
HD 219659	10 332	415	1.684	0.076	4.16	0.07	2.51	0.06	206	24	389	15	0.513	0.124
HD 222847	13 495	487	2.345	0.063	4.14	0.06	3.71	0.08	312	37	423	15	0.528	0.109
HD 223785	9628	437	1.500	0.127	4.18	0.09	2.26	0.08	209	25	383	19	0.483	0.180